Sensitivity of the LMD General Circulation Model to Greenhouse Forcing Associated with Two Different Cloud Water Parameterizations

H. Le Treut, Z.X. Li, and M. Forichon
Laboratoire de Météorologie Dynamique du CNRS, Paris, France

Postal address: LMD du CNRS; 24 rue Lhomond; 75231 PARIS cedex 05; France

Fax: (33)(1) 43 36 83 92

E-mail of H. Le Treut: letreut@lmd.ens.fr

ABSTRACT

The atmospheric General Circulation Model of the Laboratoire de Météorologie Dynamique (LMD) is coupled to a slab ocean model and is used to investigate the climatic impact of a CO_2 doubling. Two versions of the model are used with two different representations of the cloud-radiation interaction. Both of them contain a prognostic equation for the cloud liquid water content, but they differ in the treatment of the precipitation mechanism. The annual and global mean of the surface warming is similar in the two experiments in spite of regional differences. To understand the behavior of the model versions, we split the total climate change into a direct CO_2 forcing and different feedback effects (water vapor, cloud and surface albedo). The results show that, in the second model version, the cloud feedback decreases significantly, especially at high latitudes, due to an increase of low level clouds in the $2{\times}CO_2$ simulation. The modification of the cloud scheme influences also the water vapor variation and the associated feedback is reduced, in particular, over the subtropical regions. The surface albedo feedback is increased. This is due to the fact that the cloudiness is smaller over high latitudes and the surface snow is more directly exposed to incoming radiation. Although the results are qualitatively similar to the results obtained with other models, the occurrence of such compensations between different feedback mechanisms leads to a different evaluation of the overall climate sensitivity.

1. Introduction

The sensitivity of the simulated climate to a doubling of the atmospheric CO_2 content has become part of the standard evaluation of a General Circulation Model (GCM). One of the reason of the continuing interest for these experiments, in spite of the emergence of more realistic transient scenarios using fully coupled ocean-atmosphere models, is that there is still a large divergence in the appreciation of the climate sensitivity by the various existing models or by various versions of the same model (Washington and Meehl 1984; Hansen et al. 1984; Wilson and Mitchell 1987; Schlesinger and Zhao 1989; Boer et al. 1992; Senior and Mitchell 1993). Reviews of these results can be found in the IPCC reports (1990). A large part of these discrepancies can be traced back to different representations of the water vapor, ground albedo and cloud feedbacks within the models (Cess et al. 1990). As will be emphasized in Section 4, the consideration of a climate change from one equilibrium to another, as possible when considering an ocean model limited to the shallow surface layer, represents the most simple conditions to diagnose without too much ambiguity these internal feedback effects.

The role of the cloud physics in modulating the response of an atmospheric GCM to the CO_2 increase has been noted in many publications. In Wetherald and Manabe (1988), two versions of the GFDL model were compared. The results showed that the inclusion of an interactive cloud cover scheme could enhance the model sensitivity and the surface warming corresponding to a doubling of the CO_2 concentration, which increased from 3.2°C to 4.0°C. They further analysed the different feedback mechanisms in the model and showed that the cloud cover acted as a positive feedback mechanism in their model. This was due to the increase of high cloud cover near the tropopause, associated with the increase of height of the tropopause in the warming climate. It overshadowed the small negative feedback effect corresponding to increased low cloud cover at high latitudes. They also showed that the water vapor feedback was increased in the variable cloud model, that the feedback related to the variation of the temperature lapse rate was decreased, and the surface albedo feedback was almost unchanged. Mitchell and Ingram (1992) confirmed this cloud cover variation mechanism and pointed out that the cloud increase near the new tropopause and the cloud decrease below are strongly related to the vertical motions of the atmosphere. They argued that the numerical parameterization of the vertical transport of water vapor by convection and large-scale motion is critical in determining the magnitude of the cloud changes.

To take into account, in more details, the role of cloud physics in these feedback mechanisms, more comprehensive cloud schemes have been designed, where, in particular, the cloud liquid (or ice) water content was estimated by the model. The possible increase of cloud liquid water content in a warming climate could constitute a negative feedback through changes in the cloud albedo effect. The studies of Somerville and Remer (1984) with a 1-D radiative-convective model, and Roeckner et al. (1987) with a GCM, showed the potential importance of cloud liquid water content variations in regulating the climate sensitivity. The studies of Mitchell et al. (1989) and Senior and Mitchell (1993) showed in addition that the phase change between ice and water clouds may also produce a strong negative feedback and reduces the warming of the surface-troposphere system. Their studies showed also that the interactive calculation of the cloud radiative properties, by using the model produced cloud liquid water content, causes a further negative feedback. This feature is due to the fact that the dependence of cloud shortwave albedo on the cloud liquid water path is different from the dependence of cloud infrared emissivity on the cloud liquid water path, as showed in earlier studies by using simple models (Stephens and Webster 1981). However, as noted in Senior and Mitchell (1993), these additional cloud feedbacks are uncertain and may be model-dependent since our knowledge of the physical phenomena and their parameterization in large-scale models is very limited. Our results using the LMD GCM response to a prescribed change of sea surface temperature showed the crucial importance of the level at which the ice/water transition is prescribed in determining climate sensitivity (Li and Le Treut 1992).

In this paper, we review the results obtained with two versions of the atmospheric GCM developed at the Laboratoire de Météorologie Dynamique (LMD), which differ mainly through their cloud parameterizations, in response to a CO_2 doubling. In a first version we have used the cloud scheme already described in Le Treut and Li (1991). This cloud scheme is intentionally very simple, the idea of its design being to put orders of magnitude on the few parameters it contains, through a careful comparison with observed data. Two prescribed thresholds account for the ice and water precipitation mechanisms respectively. We know from the intercomparison experiments organized within the FANGIO program (Cess et al. 1990) that the model sensitivity using this cloud parameterization is rather high. As mentioned above we have repeated the $2{\times}CO_2$ sensitivity experiments with a version of the model which contains a different description of the cloud precipitation mechanism: for warm water clouds, it makes use of a simple formulation designed by Sundqvist (1981) and represents the precipitation of ice through the terminal velocity of the crystals. This parameterization of the precipitation is more reminiscent of the one used by Smith (1990). It therefore allows a more direct evaluation of our model results by comparison with other published results, in particular those of Mitchell et al. (1989) and Senior and Mitchell (1993), which revealed a dramatic decrease of the model sensitivity associated with the introduction of the Smith's (1990) cloud scheme.

The description of our model and the design of the experiments will be presented in Section 2. The basic results of the simulations will be presented in Section 3. To get some insight into the model response, and also to make the first step toward a correct validation of the model, we have tried to separate the effect of the various feedback terms. The simple method we have used, its rational, and the results obtained are described in Section 4. It was first employed in Wetherald and Manabe (1988). It considers the share of the radiative changes at the top of the atmosphere which are due to the changes in different model variables.

2. Model description and design of the experiments

a. General features.

The model used in this study, the LMD GCM, was developed in our institute (Sadourny and Laval 1984). The dynamics is formulated in finite differences. It is used here in a low resolution version of 48 points in the longitude direction, 36 points in the latitude direction, and 11 vertical layers. The physical package corresponds to one of the standard versions of the LMD GCM referenced as Cycle 4. It is described in Le Treut and Li (1991). The radiation parameterization is the same as used operationally at ECMWF (Morcrette 1991). The solar transfer scheme was originally designed by Fouquart and Bonnel (1980). The convection is represented by the combination of a moist adiabatic adjustment and a Kuo scheme. The non-convective condensation is treated through a simple statistical algorithm where a distribution of the water vapor mixing ratio inside a grid-box is considered. The cloud fraction used for the radiation is diagnosed as the fraction of the grid where condensation occurs. The liquid water formed by condensation is retained in the atmosphere as cloud water: the time evolution of this new prognostic variable is computed through a mass-balance equation. The cloud water content is then used to determine the cloud optical thickness which is needed to compute the solar fluxes and the cloud emissivity used in the infrared computation. In spite of its simplicity the model includes a large range of possible feedback processes in relation with cloud formation, which affect strongly the model sensitivity. This is not true for the surface algorithms: in this model version - in opposition with the following versions of the LMD GCM - the ground hydrology is treated with a simple bucket model, without any explicit representation of the vegetation cover, and no diurnal cycle is considered. The surface albedo over land is a function of snow depth, and is prescribed according climatological data when there is no snow cover. The surface albedo over free ocean is a function of the solar height, and the presence of sea ice is diagnosed when the sea surface temperature is below $-2°$C.

This control version of the model will be referred to as LMD4^{CO}. In the present paper we also consider a slightly modified version of this model, which differs mainly through a different representation of the precipitation process in the cloud liquid water prognostic equation and a different specification of the cloud optical properties from the knowledge of their water content. This modified version will be referred to as LMD4^{MO}.

b. Framework of cloud parameterization

To appreciate the differences in the estimation of the sensitivity obtained from the two model versions, it is necessary to describe some features of the cloud scheme used in the model. It is also described in Le Treut and Li (1991).

As already stated, the cloud water content evolution is determined through a budget equation and therefore through a simplified representation of the balance between condensation, evaporation and precipitation. The condensation is the source of the cloud water. Both convective and non-convective sources of condensation are taken into account here. The non-convective part of the condensation is taken into account through a simple statistical scheme, which uses the assumption of a uniform distribution of the total water content (vapor plus condensate) within a given grid-box, characterized by a width Δq_t. This approach implies that the water converged in a grid-box is used without distinction for the cloudy or the clear air and that condensation and evaporation are treated simultaneously. It allows the definition of a cloud fraction, as the part of the grid-surface where there is supersaturation, and consistently, the computation of a condensation rate. The choice of the width Δq_t is therefore determining. In the present simulations we have chosen $\Delta q_t = 0.2 q_t$ where q_t is the total water content. Water condensed within convective clouds is also used directly into the cloud water budget equation.

The main sink term to be parameterized is the precipitation of the cloud droplets or crystals. In our model the same precipitation process is used for both convective and non-convective cloud water, which makes a difference with other models. This precipitation term represents the effects of the micro-physical processes by which the small cloud droplets grow to relatively large rain drops, or the formation and subsequent sedimentation of the ice crystals. The main differences between LMD4^{CO} and LMD4^{MO} lie in the treatment of precipitation.

c. The treatment of precipitation

Many processes related to the large-scale dynamics or micro-physical aspects affect precipitation. The growth of cloud droplets by condensation and autoconversion, their collection by rain drops, the accretion of ice crystals are processes which will be represented through the parameterization of precipitation. A description of these processes may be found, for example, in Mason (1971), Kessler (1969) or Ludlam (1980, Ch.5). They are taken into account here in a crude statistical manner.

In LMD4^{CO}, a threshold method is used and the cloud water in excess of the threshold C_l is precipitated. We distinguish, through the cloud top temperature, two regimes of precipitation: warm water clouds and cold ice clouds. Different threshold values are chosen for the two regimes. When the cloud top temperature is warmer than -10°C, then the cloud precipitation regime is supposed to be that of water cloud with a threshold $C_l = 1 \times 10^{-4}$ kg kg^{-1}. In the contrary, if the temperature is colder than -10°C, the cloud precipitation regime is supposed to be that of an ice cloud and we chose a smaller threshold

$$C_l = \min(1 \times 10^{-5}, 0.05 q_{sat}). \tag{1}$$

where q_{sat} is the corresponding saturated water vapor mixing ratio.

In LMD4^{MO}, the precipitation mechanisms are taken into account in a different manner. A more continuous set of laws is used. For warm clouds the precipitation is parameterized using the relationship proposed by Sundqvist (1981):

$$P = C_t(1 - \exp(-(\frac{l}{C_l})^2))l \tag{2}$$

where l is the cloud liquid water mixing ratio, C_t is a time scale characteristic of the precipitation process and C_l is a threshold similar to that used in LMD4^{CO}, except that the sharp transition between non-precipitating and precipitating regimes is changed into a smoother relation. We take $C_l = 2 \times 10^{-4}$ kg kg^{-1} and $C_t = 5.5 \times 10^{-4}$ s^{-1}. Note also that l is the in-cloud liquid water content, or, equivalently, the liquid water content corresponding to total grid-box divided by the cloud fraction.

For cold clouds we use a relationship which takes into account the terminal falling speed (v) of the crystals (Starr and Cox 1985). Therefore:

$$P = \frac{l}{t} \tag{3}$$

where the time scale t is given by:

$$t = \frac{\Delta z}{v} \tag{4}$$

with Δz the depth of the model layer and (Heymsfield and Donner 1990)

$$v = 3.29(\rho l)^{0.16} \tag{5}$$

where ρ is the air density (kg m^{-3}).

d. Cloud radiative properties

In both LMD4$^{\mathrm{CO}}$ and LMD4$^{\mathrm{MO}}$, the cloud water content and the cloud fraction are interactively used in the radiation code through the calculation of cloud optical thickness (τ) and the cloud emissivity (ϵ):

$$\tau = \frac{3}{2}\frac{W}{r_e} \tag{6}$$

$$\epsilon = 1 - \exp(-\kappa W) \tag{7}$$

where W is the cloud water path (g m^{-2}), r_e is the effective radius of cloud droplets (in μm) and κ is the absorption coefficient (m^2 g^{-1}). κ was chosen as constant (0.13) in LMD4$^{\mathrm{CO}}$, but in LMD4$^{\mathrm{MO}}$, it was 0.13 for warm clouds and 0.07 for cold clouds. r_e is calculated by an empirical formula in LMD4$^{\mathrm{CO}}$:

$$r_e = 11\rho_l + 2 \tag{8}$$

where r_e is in μm and ρ_l is cloud liquid water density (in g m^{-3}) (Fouquart et al. 1990). In LMD4$^{\mathrm{MO}}$, r_e is prescribed and takes values of 10 μm and 30 μm for warm and cold clouds respectively.

e. Evaluation of the two model versions

The changes of the cloud parameterization from LMD4$^{\mathrm{CO}}$ to LMD4$^{\mathrm{MO}}$ have a large influence on the simulation of the present climate. Figure 1 shows the latitude-height diagram of the zonal mean cloud cover. At low latitudes, the cloud cover is larger in LMD4$^{\mathrm{MO}}$ than in LMD4$^{\mathrm{CO}}$. But for high latitudes, LMD4$^{\mathrm{MO}}$ has less cloud. Figure 2 shows the same diagram but for cloud liquid (or ice) water content. We can see that this quantity is sensibly increased in LMD4$^{\mathrm{MO}}$, because it is sensitive to the precipitation process. This seems more realistic compared to retrievals from SSM/I satellite observations (Wentz 1989). This indication from satellite observations is mostly qualitative, but it is the only available at the global scale. In fact the LMD4$^{\mathrm{MO}}$ model was tuned to increase the too low water content obtained for warm clouds in the LMD4$^{\mathrm{CO}}$ model. For ice clouds, the parameterization in LMD4$^{\mathrm{MO}}$ takes into account explicitly the falling velocity of ice crystals. and tends to diminish the cloud water content.

Figure 3 gives the zonal means of the cloud radiative forcing at the top of the atmosphere in LMD4^{CO} and LMD4^{MO}. Satellite observations from ERBE (for 1986) are also plotted in the figure for comparison (see Bony et al. 1992 for a more detailed and rigorous comparison with a higher resolution version of the model LMD4^{CO}). We note a clear improvement in LMD4^{MO} concerning the infrared radiation (upper panel), which probably reflects a better handling of the ice physics. In particular we may note the much better agreement obtained at high latitudes, where the cloud forcing was much reduced in LMD4^{MO} as compared to LMD4^{CO}. However, for the solar radiation component, although the global mean is close to the observation, the latitudinal variation is not sensibly improved. This is certainly related to the bad performance of our model in producing the low level marine clouds, as mentioned in Le Treut and Li (1991). Furthermore, we know that the effective radius of cloud droplets, a very important parameter in determining the cloud shortwave properties, is prescribed to a simple global value. At high latitudes, the lower absolute values in LMD4^{MO}, which are responsible for an increased importance of the surface albedo, are in agreement with the observation. The too large shortwave cloud forcing in the ITCZ is a common feature to many models.

The atmospheric moisture is also modified by the changes of cloud scheme. Figure 4(a) shows the latitude-height diagram of the changes of specific humidity (LMD4^{MO} $-$ LMD4^{CO}). The atmospheric humidity increases near the equator, because more cloud liquid water is retained in the atmosphere. On the contrary, a drying occurs in the subtropical regions, especially in the Southern Hemisphere where the drying is very strong and extends to relatively high latitudes. In the high latitudes of both hemispheres, the atmospheric humidity increases, also due to the large amount of cloud liquid water being retained in the atmosphere. Figure 4(b) shows the latitudinal variation of the vertically integrated water vapor in LMD4^{CO} and LMD4^{MO}. Compared to the observation (Oort 1983), both versions of the model are too dry in the tropics. Near the equator the higher values in LMD4^{MO} appear as an improvement. In the subtropics reversly the model LMD4^{CO} is closer to the observation.

f. Design of the sensitivity experiments

The perturbation of the climate due to a doubling of the CO_2 is computed using a simple description of the ocean as a slab layer. The technique is the same as used by several other groups (Hansen et al. 1984; Wilson and Mitchell 1987; Boer et al. 1992). The evolution of the sea surface temperature (SST or noted as T_{sst}) is governed by the following equation:

$$C\frac{\partial T_{sst}}{\partial t} = F + T \tag{9}$$

where C is the heat capacity of the ocean which depends on the depth of the slab layer, and T the transport of energy by the ocean. We first realize a control simulation with prescribed SSTs as given by observations and we diagnose the associated surface fluxes (F), which yields an estimation of the oceanic heat transport (T). For a perturbed climate we assume that the transport T is unchanged: this is an unrealistic but necessary assumption in the absence of any representation of the ocean dynamics. Therefore the evolution equation for the SST in the perturbed experiment is:

$$C\frac{\partial(\Delta T_{sst})}{\partial t} = \Delta F \tag{10}$$

where the increment ΔF refers to the difference in fluxes between the perturbed experiment and the control experiment (realized using climatological SSTs), and ΔT_{sst} is the difference between the SSTs of the perturbed climate and the prescribed climatological SSTs.

This simple representation of the ocean therefore consists in calculating the perturbation of the SSTs. It allows us to evaluate the climate sensitivity to a given perturbation by providing a simple closure for the various feedback mechanisms including surface temperature. But it is important to note that if we now try to use this approach to simulate again the present climate, the results are affected by a systematic bias, when compared to the simulation using prescribed SSTs. This may come as a surprise because setting $\Delta F = 0$ in equation (10) implies that $\Delta T_{sst} = 0$ and the two simulations with prescribed and computed SSTs should then give exactly the same results. This behavior appears in fact because equation (10) is not applied at each model time step, but every day. This is done because ΔF represents the ocean transport, not a correction term, and is evaluated using a reference which is filtered in time. This leads to a decorrelation between the two atmospheric simulations with calculated and prescribed SSTs. The fact that this very simple coupled model can drift away from its reference climate is not particular to our model, but is worth being stressed because it indicates some intrinsic instability of the ocean/atmosphere coupling. Figure 5 shows the geographical distributions of the surface temperature changes between the two simulations for both the LMD4$^{\mathrm{CO}}$ and LMD4$^{\mathrm{MO}}$ models. We can see that an oscillation structure is clearly present, especially at high latitudes of the Southern Hemisphere (three maxima and minima).

We have integrated twice the model with equation (10), for present conditions (CO_2 level is 320 ppm) and double CO_2 conditions (CO_2 level is 640 ppm). We have therefore run three experiments: (*a*) a control experiment with prescribed SSTs (we will refer to it as $1\times CO_2$p) (*b*) a control experiment with simulated SSTs (we will refer to it as $1\times CO_2$) (*c*) a perturbed experiment with simulated SSTs (we will refer to it as $2\times CO_2$)

3. Main results of the simulated climate change

a. Global average

The temporal evolution of the global mean SSTs is displayed in Figure 6 for all experiments with the LMD4^{CO} and LMD4^{MO} versions. Note that the depth of the slab ocean is chosen as 50 m - value suggested by Manabe and Stouffer (1980) to produce a correct seasonal cycle. However, in LMD4^{CO}, this depth was reduced to 20 m during the first ten years in order to accelerate the model convergence and gain computer time. This explains why, in Figure 6, LMD4^{CO} tends to equilibrium more rapidly. In another study not reported here, we have checked that the reduction of the slab ocean depth in approaching the equilibrium had no notable impact on the equilibrium climate itself. In the present paper, all the results are obtained by using the last ten years of the simulations.

Figure 6 reveals that, as already stated, there is a systematic drift between the $1\times CO_2$ and $1\times CO_2$p experiments. It occurs for both model versions, although with a different amplitude. If we evaluate the climate change by using $1\times CO_2$p and $2\times CO_2$, the global warming should be 5.4°C and 4.3°C for respectively LMD4^{CO} and LMD4^{MO}. However it is more consistent to evaluate the climate change by using $1\times CO_2$ and $2\times CO_2$, since these two simulations are realized under exactly the same conditions, except for the CO_2 concentration. The global warming so obtained is 3.9°C for the LMD4^{CO} model, and 3.6°C for the LMD4^{MO} model.

Table 1 presents the global and annual averages of the main climate parameters in the $1\times CO_2$ and $2\times CO_2$ simulations for both versions of the model. Also tabulated are the changes from $1\times CO_2$ to $2\times CO_2$.

We see that, as the global temperature, the precipitation increases in both experiments, which indicates an intensification of the hydrological cycle in a warm climate. The increase is 0.25 mm day^{-1} for LMD4^{CO} and 0.17 mm day^{-1} for LMD4^{MO}. This represents a relative increase of 8% and 5% respectively.

The changes of water vapor in the atmosphere are very large and they reach up to 31% in LMD4^{CO} and 29% in LMD4^{MO}. The important increase of water vapor content in a warm climate, also reported by other groups, is largely the manifestation of the Clausius-Clapeyron equation.

The cloud cover decreases in both experiments, more notably in LMD4^{CO} (2%) than in LMD4^{MO} (1%). This feature of our model again agrees with most other models (Wetherald and

Manabe 1988; Mitchell and Ingram 1992; Boer et al. 1992). The cloud liquid water content is almost unchanged in LMD4^{CO}, but it increases in LMD4^{MO} (6.8%).

The decrease of the surface albedo is 0.45% in LMD4^{CO} and 0.65% in LMD4^{MO}. This variation of surface albedo is essentially due to the melting of snow cover and sea ice. Figure 7 shows the zonally averaged changes of surface albedo. We can see that the decrease for the Northern Hemisphere is similar in the two experiments. However, for the Southern Hemisphere, the decrease is more important for LMD4^{MO}, which is certainly related to the fact that in these regions the cloudiness is smaller and the surface warming is larger in LMD4^{MO} (Figure 8).

b. Geographical distribution

Maps of the mean annual surface warming are shown in Figure 8 for the two experiments. We have added the results of a third experiment (Nesme-Ribes et al. 1993) which studies the model response to a 4 W m^{-2} increase in the mean insolation, with the LMD4^{CO} model. First of all, we can note that the response of the model to a global forcing of different nature (CO_2 increase versus solar constant increase), is almost unchanged, whereas the change from one cloud parameterization to the other leads to more important variations in the geographical distribution of the warming.

For both experiments LMD4^{CO} and LMD4^{MO}, the warming is smaller in the intertropical regions over the ocean and is larger at high latitudes, where the melting of snow or sea ice occurs. If we examine the zonal variations of the surface warming at high latitudes, the structure in the Southern Hemisphere is very similar for the two experiments, with three or four maxima. For the Northern Hemisphere, the temperature changes over North America are very similar in the two experiments. However, the situation is quite different over the Eurasian continent. In LMD4^{CO}, the Central Asia is warmer by more than 5°C whereas the warming over Europe is very small, even less than 1°C. However, in LMD4^{MO}, the warming over the central part of the continent is less than 4°C and the maximum warming (more than 7°C) is over Europe. The minimum warming center is now pushed to North Atlantic, near Greenland.

The changes in the precipitation field for both models are shown in Figure 9 (upper and middle panels). Again our results are consistent with other already published results. Large modifications occur over the intertropical regions, where they seem related to shifts in the position of the ascending branches of the Hadley-Walker circulation. Weaker modifications at mid-latitudes correspond to a rather systematic increase of the precipitation. We have added in Figure 9 (lower panel) a plot in which the change in mean annual precipitation obtained for

$LMD4^{MO}$ is normalized by the interannual variability of the precipitation (as estimated from 10-year series for both the $1{\times}CO_2$ and $2{\times}CO_2$ experiments). The response at high latitudes is much more significant. We know that the increase of water transport to these regions gives a moistening of the lower atmosphere in response to the warming.

The seasonal distribution of the warming and the changes of precipitation may be seen in Figure 10 for the experiment $LMD4^{MO}$ (it is qualitatively similar for the experiment $LMD4^{CO}$). The model, as most other models, amplifies the warming in winter at high latitudes, whereas the warming in the intertropical region remains constant throughout the annual cycle. The precipitation increases along the equator and two bands of decreased precipitation can be noted in the subtropical regions. We can also observe a latitudinal shift of the precipitation structure with the seasons, especially in the Northern Hemisphere.

c. Changes in the mean zonal climate

We have gathered, in Figures 11, 12, 13, 14 and 15 respectively, information on the mean zonal response in terms of temperature, water vapor (absolute and relative variations), cloudiness and cloud condensed water content. The upper panel corresponds to $LMD4^{CO}$, and the lower panel to $LMD4^{MO}$. The results are, for both model versions, in qualitative agreement with those of other models (Schlesinger and Mitchell 1987; IPCC 1990).

Concerning the temperature changes (Figure 11), we may note the occurrence of usual features, namely, a cooling in the stratosphere and a general warming in the troposphere and near the surface. The tropospheric warming is maximum near the tropopause at low latitudes for both experiments. This feature is consistent with the results obtained in simulations using a penetrative convection scheme (Wilson and Mitchell 1987; Hansen et al. 1984). It probably means that, in our model, even if the largest share of the precipitation is taken by the moist adjustment, the Kuo scheme is efficient in propagating the warming up to the higher levels of the troposphere. We can also note some differences between $LMD4^{CO}$ and $LMD4^{MO}$: in particular, the tropopause warming over the tropical regions is more important in $LMD4^{MO}$, which is certainly related to the intensification of the moisture processes. In high latitudes, the warming of the lower layers of the atmosphere is restricted to lower levels in $LMD4^{MO}$ than in $LMD4^{CO}$.

The increase of the atmospheric humidity in the atmosphere is a close reflection of the temperature increase, as the atmospheric humidity in the actual atmosphere is largely dependent on the temperature structure. The absolute values of increase are large at the surface near the equator and they decrease with latitude and altitude, as shown in Figure 12. The water vapor changes are mostly apparent in the low latitude regions where the water vapor saturation value is also higher. We may note that in the LMD4$^{\mathrm{MO}}$ case the water vapor increase is smaller in the subtropical regions. This reflects the fact that, for the simulation of the present climate, the LMD4$^{\mathrm{MO}}$ model simulates differently the low latitude clouds: they contain more water than in the LMD4$^{\mathrm{CO}}$ model, they form a better organized cloud band along the ITCZ, and, reversely, the subtropical areas are drier. Incidentally this means that a change in the micro-physical part of the model is able to bring large changes in the large-scale organization of the precipitation. The relative increase of the specific humidity (e.g. the increase scaled by the value of q itself), shown in Figure 13, is maximum near the tropopause. This feature is consistent with the results presented by Mitchell and Ingram (1992).

For both LMD4$^{\mathrm{CO}}$ and LMD4$^{\mathrm{MO}}$, the cloudiness (Figure 14) generally decreases in the model lower layers (below 300 mb), which reflects a decrease of the relative humidity due to the warming, and increases in the high layers (above 300 mb), as also occurs in many models. However, a more careful examination shows that the main differences between LMD4$^{\mathrm{CO}}$ and LMD4$^{\mathrm{MO}}$ occur near the transition region between water and ice, where LMD4$^{\mathrm{MO}}$ presents an increase in cloudiness, due to the replacement of ice clouds by water clouds (Mitchell et al. 1989; Senior and Mitchell 1993). LMD4$^{\mathrm{CO}}$ does not present a progressive transition zone, and does not show this feature of cloudiness increase in the troposphere. This difference is particularly evident at high latitudes near the surface where most regions of cloudiness diminution in LMD4$^{\mathrm{CO}}$ disappear in LMD4$^{\mathrm{MO}}$. However, compared to the results of Mitchell et al. (1989), this increase of cloudiness near the water-ice transition zone in LMD4$^{\mathrm{MO}}$ is smaller, which is certainly related to the fact that the contrast between water and ice clouds is also smaller in our model. All these features are clearly associated with the cloud schemes. As we changed our criteria to define when a cloud is precipitating following the Bergeron process, from a non-local one in LMD4$^{\mathrm{CO}}$ (cloud top below $-10°$C) to a local one in LMD4$^{\mathrm{MO}}$ (cloud layer below $-15°$C), we also changed very strongly the location of the cloud water increase associated with the transition from liquid water to ice in the case of a warming (Li and Le Treut 1992).

Concerning the changes in cloud liquid water content (shown in Figure 15), we note that the amplitude of increase or decrease in LMD4$^{\mathrm{CO}}$ is less important since the initial values are smaller in this version of the model. The general feature is that clouds thicken at high altitudes and get thinner at low altitudes, except for the regions near South Pole. The structure of cloud water content changes obtained with the $LMD4^{MO}$ model are very reminiscent of that obtained by Mitchell et al. (1989) using the UKMO model, which is consistent with the fact that the cloud scheme of $LMD4^{MO}$ is rather similar to the cloud scheme of Smith (1990) used by Mitchell et al. (1989). We may also note that there is more consistency between the cloud water content and cloudiness changes in the $LMD4^{MO}$ than in the $LMD4^{CO}$ model, which certainly reflects the replacement of a precipitation mechanism using prescribed thresholds, in $LMD4^{CO}$, by a more continuous one in $LMD4^{MO}$.

Finally we close this description of the changes in the zonally averaged climate of the model by showing the stream-function of the mean circulation of July for the present climate, and for the $2\times CO_2$ climate (shown in Figure 16 for the $LMD4^{CO}$ case only, because both experiments give results which are qualitatively similar). We see a weakening of the Hadley cell, which is mainly associated with the decrease of the temperature gradient at the lower layers of the atmosphere between low and high latitudes. However, the Hadley cell seems to have a larger extension, probably due to the increase of equator-pole temperature gradient in the upper layers of the troposphere. As discussed in more details in Nesme-Ribes et al. (1993) for the (very similar) case of a change in the solar constant, we may note that we get in the case of the $2\times CO_2$ forcing a reduction of the poleward transport of (air) mass and energy, but an increase of the water vapor transport, necessary to get the extratropical increase in precipitation already noted. This latter effect is due to the overcompensation of the Hadley cell weakening by the water vapor increase.

4. Diagnostics of the main feedback effects

a. General formulation

The response of the climate system to a CO_2 increase may be viewed as a direct thermal response to an additional radiative forcing, amplified by a few feedback mechanisms which are related to the variations of the internal variables of the climate system (Hansen et al. 1984, Schlesinger 1988). It is useful to split a climate change effect into different terms of forcing and feedbacks. We assume that the radiation budget R at the top of the atmosphere depends on an "external" parameter λ (here λ is the atmospheric CO_2 content), the surface temperature T_s and the internal parameters x_i (temperature, water vapor, albedo). At equilibrium,

$$R(\lambda, T_s, x_i) = 0 \tag{11}$$

If we move from one equilibrium state to another:

$$\delta R = \frac{\partial R}{\partial \lambda}\delta\lambda + \frac{\partial R}{\partial T_s}\delta T_s + \sum \frac{\partial R}{\partial x_i}\delta x_i = 0 \tag{12}$$

which yields a relation between δT_s and the forcing $\frac{\partial R}{\partial \lambda}\delta\lambda$:

$$\delta T_s = \frac{\frac{\partial R}{\partial \lambda}\delta\lambda}{-\frac{\partial R}{\partial T_s}|_{x_i} - \sum \frac{\partial R}{\partial x_i}\frac{\delta x_i}{\delta T_s}} \tag{13}$$

The first term in the denominator is a first-order sensitivity term; the other terms, related to x_i, may be called "feedback terms".

This interpretation is valid primarily when R is the globally averaged radiative budget. But we may extend it to local changes and we compute, in the following section, the zonal mean distribution of $\frac{\partial R}{\partial x_i}\delta x_i$ to asses the contribution from the different parameters at different latitudes.

The simulations undertaken here provide a good framework to use such a formalism, since they are equilibrium experiments (as opposed to the a priori more realistic transient simulations of the climate response to a slowly increasing greenhouse forcing).

To evaluate the climate feedbacks, one could also realize several parallel experiments in which the variables of the system would be fixed one after the other. This approach requires a great number of simulations and is technically difficult due to the interaction of various processes in a model. Hansen et al. (1984) have done such a study using a 1-D model in order to diagnose the feedback mechanisms of their GCM. As noted in Wetherald and Manabe (1988), the sensitivities obtained by the 1-D model could be significantly different from those of the GCM. In particular, it is difficult to determine a global mean cloudiness with the same radiative effect as in a 3-D model.

The radiative forcing associated with a CO_2 doubling might be appropriately described as a forcing exerted at the tropopause, since the stratosphere is on the contrary cooling itself. Yet the difficulty to diagnose the tropopause level in standard model outputs, and the validation opportunities offered by satellite data make it more convenient to consider the forcing and the amplifying terms at the top of the atmosphere. We may also note that, when using a slab ocean, the heat gained by the climatic system, which is mainly the one stored by the ocean, is directly reflected in the slab ocean mean temperature, and therefore in the surface temperature. Therefore the relation between the fluxes at the top of the atmosphere and the surface temperature offer a description of the model sensitivity (Cess and Potter 1988) which is well adapted to our simulations.

We now want to isolate the contributions of different variables to changes in the radiative budget at the top of the atmosphere. If we note R the mean radiative budget of the atmosphere, which depends on parameters $(x_1, ..., x_i, ..., x_n)$, we define the changes of R associated to the parameter x_i as:

$$\Delta R_i = R\left(x_1^1, ..., x_i^2, ..., x_n^1\right) - R\left(x_1^1, ..., x_i^1, ..., x_n^1\right) \qquad (14)$$

the superscripts ^{2} or ^{1} referring to the experiment for the $2\times CO_2$ climate or for the present climate respectively. There are no a priori reasons to believe that the various contributions correspond to linear and independent processes, which means that the modifications in the global radiative budget arising from changes in temperature, water vapor, cloud parameters or surface albedo are not necessarily balanced. This is reinforced by the fact that we used monthly means to do our radiative computations. The global energy balance proves however a posteriori to be roughly true. But we should interpret our results as being indicative only, and as a diagnostic tool to compare the two model versions. Some processes are definitely not independent. We found for example impossible to isolate through this diagnostic method the effects of the cloud fraction and cloud optical thickness, because of the strong link between those two parameters. A clear diagnosis of the cloud optical thickness feedback would be very important (Li and Le Treut 1992) but could not be performed unambiguously.

b. Results of feedback analysis

The results of this feedback analysis for the two model versions are given in Figure 17 in the form of zonal average. The direct forcing resulting from CO_2 doubling is rather uniform with slightly larger values in the tropical and sub-tropical regions. However we can observe a decrease near the equator, which is certainly related to the activity of the ITCZ, diminishing the direct forcing of increased CO_2. From a global point of view, we can note the positive sign of the water vapor, cloud and surface albedo feedbacks.

The water vapor feedback is very strong in the two versions of our model. Its effect is generally reduced by a change in the temperature lapse-rate (Duvel et al. 1992), which is not shown here, since all temperature effects are considered to be part of the "no-feedback" response in our decomposition. It is slightly modified from one experiment to the other. The most noticeable modification is a decrease in the subtropical regions of the Southern Hemisphere for the experiment LMD4^{MO}. This is consistent with the fact that in this experiment the water vapor content (for the control climate) is diminished in the subtropical areas: the water vapor increase is also diminished. The water vapor feedback being very strong in the climate system, its good representation in climate models is important to get a correct model sensitivity. Certainly, the variation of water vapor is, at first order, controlled by the atmospheric temperature, but also by the circulations of different scales. As shown by Emanuel (1991), the representation of the microphysical aspects of clouds can influence dramatically the water vapor distribution and changes, and therefore the water vapor feedback.

Validating the water vapor (and temperature lapse-rate) feedback in our GCM has been the subject of various studies. One approach is to consider the seasonal cycle. The studies undertaken presently (see Duvel et al. 1992 for early results) show that the water vapor sensitivity at mid-latitudes is mainly a reflection of the temperature structure of the atmosphere, whereas in the tropics it is more dependent on the parameterization of the hydrological cycle and on the large-scale atmospheric circulation. A large sensitivity of the model in the intertropical regions is apparent. However the sensitivity deduced at the seasonal time scale is different from that associated with the greenhouse warming, and this requires further studies.

The largest modifications between the two experiments concern the cloud effect. In the LMD4^{CO} experiment we have positive cloud feedback, almost uniformly over the globe, with smaller values in the tropics. This can be easily understood from the mean zonal response shown in Figures 14 and 15. In LMD4^{CO} the cloud response can be described by distinguishing three vertical layers, which have little latitudinal dependence, as follows: under 500 mb, roughly, a decrease of both cloud cover and cloud water content; between 500 and 200 mb, a decrease of cloud cover but an increase of cloud water content associated to the transition between ice and liquid water clouds; above 200 mb, an increase of both cloud cover and cloud water content. The increase of cloud water content at high levels is certainly linked to the fact that for ice clouds the precipitation threshold depends on the local temperature, because it is prescribed as a fraction of the water vapor saturation value. This leads to a positive feedback, whose magnitude is very dependent on the height (or temperature) at which the ice/water transition is prescribed (Li and Le Treut 1992). On the contrary in the LMD4^{MO} experiment this layering is valid in the Tropics only, where we get accordingly a rather strong positive feedback associated with cloudiness. At high latitudes we have deep changes: the use of a continuous precipitation law, rather than a prescribed threshold, has brought much more consistency between the cloud cover and cloud water content changes. We have now a low level cloud increase and cloud thickening, very reminiscent of the features shown by the UKMO model (Mitchell et al. 1989), which brings, as in the UKMO experiments, a negative feedback.

The feedback related to the surface albedo is visible in the high latitudes of the two Hemispheres. It increases in the LMD4^{MO} model. One reason to explain this feature is that the cloud cover is less important in LMD4^{MO} at the high latitudes, and the albedo effect is more effective since more solar energy reaches the ground. This is an example of interaction between two feedback mechanisms (we can call it a second order feedback). Another reason, especially in the Southern Hemisphere, is the strong decrease of the mean surface albedo due to a surface warming in LMD4^{MO} (Figure 7).

We know that the surface temperature is a good indicator of the climate system, especially in those experiments where it is also the temperature of the slab ocean, and the variations of the radiative budget at the top of the atmosphere represent an adequate quantity to compare the direct forcing and different feedbacks. It is therefore informative to split the surface warming ($\Delta T_s^{\text{total}}$) into terms of forcing (ΔT_s^i, where i represents CO_2) and feedbacks (ΔT_s^i, where i represents respectively the feedbacks related to water vapor, cloud and surface albedo) by using:

$$\Delta T_s^i = \Delta T_s^{\text{total}} \times \Delta R_i / (\sum_{i=1}^{4} \Delta R_i) \tag{15}$$

The results are tabulated in Table 2 and constitute a rough but quantitative method to compare LMD4^{CO} and LMD4^{MO}. The direct warming due to the CO_2 doubling is similar in LMD4^{CO} and LMD4^{MO}: 0.64°C and 0.61°C respectively. Note that these values would not represent the surface warming for a $2\times CO_2$ scenario without any feedback (which is generally considered as 1.2°C). We use here the radiative budget at the top of the atmosphere and the direct forcing of CO_2 increase is less than the value at the tropopause due to the stratospheric temperature inversion (Schlesinger 1988). Again changes in the temperature lapse-rate are not considered in this simple approach. From Table 2, we can see that the contribution of the water vapor changes is 2.52°C in the experiment LMD4^{CO}, and decreases to 2.26°C in LMD4^{MO}, mainly due to the decrease of water vapor changes in the subtropical regions. The contribution of the cloud feedback also diminishes from LMD4^{CO} to LMD4^{MO} (0.62°C to 0.42°C), mainly due to the negative contribution at high latitudes. On the contrary, the contribution of surface albedo feedback increases.

If the overall warming in the experiment LMD4^{MO} remains rather large (3.6°C compared to 3.9°C in the LMD4^{CO} experiment), this seems due to two factors: the strong positive cloud feedback in the tropics, and an increase of the high latitude albedo feedback, which tends to compensate the corresponding decrease in the cloud feedback term in high latitudes. These two effects may be very model dependent. First the cloud response in the Tropics is largely due to the anvils of the convective clouds, whose parameterization is rather uncertain, as is the coupling of convective and non-convective cloud regimes in most models. Then the change in the effect of the surface albedo at high latitudes depends very much on the parameterization of the vegetation and also reflects the characteristics of the mean cloud climatology, because we are considering the impact of the surface albedo on the radiation budget at the top of the atmosphere.

5. Summary and Conclusion

We have examined two versions of the LMD GCM where the mechanism of the cloud water precipitation was treated differently. Slight modification in the specification of the cloud optical properties from the simulated water content were also introduced. In $LMD4^{CO}$, a simple threshold method was used and the distinction of ice clouds from water clouds was based on the cloud top temperature. In $LMD4^{MO}$, this distinction was made by using the local atmospheric temperature. Furthermore, the precipitation of water clouds was based on a smoother formula and that of ice clouds took into account explicitly the falling velocity of ice crystals. The direct consequences of these modifications are the following: the cloudiness decreases at high latitudes but it increases in the intertropical regions; the cloud liquid water content increases considerably, especially at low latitudes near the equator. The atmospheric humidity has also been changed by the modifications of the cloud scheme. A large increase of water vapor is found in the tropics but a decrease takes place in the subtropical regions.

Our GCM has been coupled to a slab ocean model, and we have done two standard CO_2 doubling experiments with the two different cloud schemes. The main results are consistent with those of the other groups who have done the same simulations. The surface warming is minimum over the tropical oceanic regions and it increases at high latitudes. The geographical distribution of the surface warming is similar in the two experiments, except for the North Atlantic and Eurasian continent. But the natural variability over these regions is large, and certainly amplified by our simple treatment of the ocean. The pattern of precipitation changes is also consistent with other groups: increase of precipitation at high latitudes due to the intensification of the water vapor transport by the atmosphere. For the subtropical dry regions, the precipitation decreases further, even if the Hadley cell seems weakened in the $2{\times}CO_2$ scenario. This feature is due to the decrease of relative humidity in these regions. The convection activity of the ITCZ seems intensified and the associated precipitation increases. However, the geographical location of this intensification is highly uncertain, since the variability is large.

The main interest of these simulations is to show that, if the model version called here $LMD4^{MO}$ presents a cloud scheme very similar to the one used by Senior and Mitchell (1993), with a change in the cloud cover and cloud water content in response to a CO_2 doubling also similar qualitatively, the impact on the climate sensitivity is nevertheless different. Indeed, in spite of very strong changes in the nature of the cloud feedbacks, the overall sensitivity of the model has remained little affected (the annual averaged global surface warming is 3.6°C in $LMD4^{MO}$ against 3.9°C in $LMD4^{CO}$). To understand this result, we have applied a procedure of feedback analyses, which consists in evaluating the contributions of different internal variables to the changes of the radiative budget at the top of the atmosphere. Certainly, this method (Wetherald and Manabe 1988) provides an artificial split between a "forcing" and some "response" terms, but it gives a quantitative element of comparison of different effects, especially useful to compare two similar experiments. The results show that, globally, the water vapor feedback, cloud feedback and surface albedo feedback are all positive ones in the two model versions. The water vapor feedback is reduced for the subtropical regions by the modified cloud scheme in the $LMD4^{MO}$ version. The changes of the cloud feedback between the two model versions are the most important. We get a negative cloud feedback at high latitudes in the $LMD4^{MO}$ model, due to an increase of low level clouds between the present and the $2{\times}CO_2$ climates. However this decrease of climate sensitivity is almost compensated by the increase of the surface albedo feedback, which is intensified in $LMD4^{MO}$ since the clouds were less at high latitudes and the surface albedo, which is larger, is also more effective. The decrease of the surface albedo for the Southern Hemisphere in $LMD4^{MO}$ is also more important due to a more efficient melting of sea ice.

The results obtained in this paper give an indication on the necessary steps to reach a reliable prediction of climate change by existing models. First, model intercomparisons must be oriented toward a detailed assessment of the various feedback effects: a global assessment is clearly insufficient because of the compensation effects noted in our results. The diagnosis of the feedback effects should be assessed from observations, for the natural variability of climate. Unfortunately the seasonal cycle, the interannual variability, while they are documented with a good precision for most of the variables considered in our study, are poor substitutes of a CO_2 doubling, because they are mainly characterized by strong horizontal shift of the meteorological structures, and because no equilibrium or quasi-equilibrium is ever achieved. This is why "integrated" measures of the climate sensitivity through the study of long-term climate fluctuations (paleoclimates, little ice age) are also useful. They constitute the only changes in which the interaction between the various atmospheric feedbacks was primarily triggered by important changes in the vertical stratification of the atmosphere.

Acknowledgments. We thank Rémi Butel who contributed to the model development and optimization. We also thank Robert Sadourny for many useful discussions on climate sensitivity analysis. This work is partly supported by the EC (European Commission) and the PNEDC (French national climate programme). Numerical experiments were run at CCVR (Centre de Calcul Vectoriel pour la Recherche).

REFERENCES

Boer, G.J., N.A. McFarlane, and M. Lazare, 1992: Greenhouse gas-induced climate change simulated with the CCC second-generation general circulation model. *J. of Climate*, **5**, 1045-1077.

Bony, S., H. Le Treut, J.P. Duvel, and R. Kandel, 1992: Satellite validation of GCM-simulated annual cycle of the earth radiation budget and cloud forcing. *J. Geophys. Res.*, **97D**, 18061-18081.

Cess, R.D., and G.L. Potter, 1988: A methodology for understanding and intercomparing atmospheric climate feedback processes in general circulation models. *J. Geophys. Res.*, **93**, 8305-8314.

Cess, R.D., G.L. Potter, J.P.Blanchet, G.J. Boer, A.D. Del Genio, M. Déqué, V. Dymnikov, V. Galin, W.L. Gates, S.J. Ghan, J.T. Kiehl, A.A. Lacis, H. Le Treut, Z.X. Li, X.Z. Liang, B.J. McAvaney, V.P. Meleshko, J.F.B. Mitchell, J.J. Morcrette, D.A. Randall, L. Rikus, E. Roeckner, J.F. Royer, U. Schlese, D.A. Sheinin, A. Slingo, A.P. Sokolov, K.E. Taylor, W.M. Washington, R.T. Wetherald, I. Yagai, and M.H. Zhang, 1990: Intercomparison and interpretation of climate feedback processes in 19 atmospheric general circulation models. *J. Geophys. Res.*, **95D**, 16601-16615.

Duvel, J.P., R. Kandel, S. Bony, and H. Le Treut, 1992: Relation between the precipitable water and greenhouse effect: lapse rate influence. *Proceedings of the IRS'92.*

Emanuel, K.A., 1991: A scheme for representing cumulus convection in large-scale models. *J. Atmos. Sci.*, **48**, 2313-2335.

Fouquart, Y., and B. Bonnel, 1980: Computations of solar heating of the Earth's atmosphere: A new parameterization. *Beitr. Phys. Atmosph.*, **53**, 35-62.

Fouquart, Y., J.C. Buriez, M. Herman, and R.S. Kandel, 1990: The influence of clouds on radiation: A climate-modelling perspective. *Rev. Geophys.*, **28**, 145-166.

Hansen, J., A. Lacis, D. Rind, G. Russell, P. Stone, I. Fung, R. Ruedy, and J. Lerner, 1984: Climate sensitivity: analysis of feedback mechanisms. in *Climate process and climate sensitivity* (Eds.: J.E. Hansen, T. Takahashi), Maurice Ewing Series (5), Amer. Geophys. Union, 130-163.

Heymsfield, A.J., and L.J. Donner, 1990: A scheme for parameterizing ice-cloud water content in general circulation models. *J. Atmos. Sci.*, **47**, 1865-1877.

IPCC (Intergovernmental Panel on Climate Change), 1990: Equilibrium climate change - and its implications for the future (Chapter 5) in *Climate change, the IPCC scientific assessment.* World Meteorological Organization, United Nations Environmental Program, Geneva, published by Cambridge University Press, 131-172.

Kessler, E., 1969: *On the distribution and continuity of water substance in atmospheric circulations.* American Meteorological Society Monographs, Volume 10, Number 32, Boston, 84 pp.

Kuo, H.L., 1965: On formation and intensification of tropical cyclones through latent heat release by cumulus convection. *J. Atmos. Sci.*, **22**, 1482-1497.

Le Treut, H., and Z.X. Li, 1991: Sensitivity of an atmospheric general circulation model to prescribed SST changes: feedback effects associated with the simulation of cloud optical properties. *Climate Dyn.*, **5**, 175-187.

Li, Z.X., and H. Le Treut, 1992: Cloud-radiation feedbacks in a general circulation model and their dependence on cloud modelling assumptions. *Climate Dyn.*, **7**, 133-139.

Ludlam, F.H., 1980: The formation, growth, and evaporation of cloud particles (Chapter 5) in *Clouds and storms, the behavior and effect of water in the atmosphere.* The Pennsylvania State University Press, 82-112.

Manabe, S., and R.J. Stouffer, 1980: Sensitivity of a global climate model to an increase in the CO_2 concentration in the atmosphere. *J. Geophys. Res.*, **85**, 5529-5554.

Mason, B.J., 1971: *The physics of clouds*, 2nd ed., Clarendon Press, Oxford, 671 pp.

Mitchell, J.F.B., C.A. Senior, and W.J. Ingram, 1989: CO_2 and climate: A missing feedback ?. *nature*, **341**, 132-134.

Mitchell, J.F.B., and W.J. Ingram, 1992: Carbon dioxide and climate: mechanisms of changes in cloud. *J. of Climate*, **5**, 5-21.

Morcrette, J.J., 1991: Radiation and cloud radiative properties in the ECMWF operational weather forecast model. *J. Geophys. Res.*, **96D**, 9121-9132.

Nesme-Ribes E., E.N. Ferreira, R. Sadourny, H. Le Treut, and Z.X. Li, 1993: Solar dynamics and its impact on solar irradiance and the terrestrial climate. *J. of Geophys. Res.*, **98A**, 18923-18935.

Oort, A.H., 1983: Global atmospheric circulation statistics 1958-1973, NOAA Professional Paper No.14, U.S. Government Printing Office, Washington D.C., 180 pp + 47 microfiches.

Ramanathan, V., R.D. Cess, E.F. Harrison, P. Minnis, B.R. Barkstrom, E. Ahmad, and D. Hartmann, 1989: Cloud-radiative forcing and climate: results from the Earth Radiation Budget Experiment. *Science*, **243**, 57-63.

Roeckner, E., U. Schlese, J. Biercamp, and P. Loewe, 1987: Cloud optical depth feedbacks and climate modelling. *Nature*, **329**, 138-140.

Sadourny, R., and K. Laval, 1984: January and July performance of the LMD general circulation model. in *New perspectives in climate modelling*, (Eds.: A. Berger, C. Nicolis), Elsevier, 173-198.

Senior, C.A., and J.F.B. Mitchell, 1993: Carbon dioxide and climate: the impact of cloud parameterization. *J. of Climate*, **6**, 393-418.

Schlesinger, M.E., 1988: Quantitative analysis of feedbacks in climate model simulations of CO_2-induced warming. in *Physically-based modelling and simulation of climate and climatic change, Part 2*, (Ed.: M.E. Schlesinger), NATO ASI series (C243), 653-735.

Schlesinger, M.E., and J.F.B. Mitchell, 1987: Climate model simulations of the equilibrium climatic response to increased carbon dioxide. *Rev. Geophys.*, **25**, 760-798.

Schlesinger, M.E., and Z. Zhao, 1989: Seasonal climate changes induced by doubled CO_2 as simulated by the OSU atmospheric GCM / mixed-layer model. *J. of Climate*, **2**, 459-495.

Smith, R.N.B., 1990: A scheme for predicting layer cloud and their water content in a general circulation model. *Quart. J. Roy. Meteor. Soc.*, **116**, 435-460.

Somerville, R.C.J., and L.A. Remer, 1984: Cloud optical thickness feedbacks in the CO_2 climate problem. *J. Geophys. Res.*, **89**, 9668-9672.

Starr, D.O'C., and S.K. Cox, 1985: Cirrus clouds. Part I: a cirrus cloud model. *J. Atmos. Sci.*, **42**, 2663-2681.

Stephens, G.L., and P.J. Webster, 1981: Clouds and climate: sensitivity of simple systems. *J. Atmos. Sci.*, **38**, 235-247.

Sundqvist, H., 1981: Prediction of stratiform clouds: results of a 5-day forecast with a global model. *Tellus*, **33**, 242-253.

Washington, W.M., and G.A. Meehl, 1984: Seasonal cycle experiment on the climate sensitivity due to a doubling of CO_2 with an atmospheric general circulation model coupled to a simple mixed layer ocean model. *J. Geophys. Res.*, **89**, 9475-9503.

Wentz, F.J., 1989: User's manual, SSM/I Geophysical tapes, Remote sensing systems, Tech Rep. No. 060989, 16pp.

Wetherald, R.T., and S. Manabe, 1988: Cloud feedback processes in a general circulation model. *J. Atmos. Sci.*, **45**, 1397-1415.

Wilson, C.A., and J.F.B. Mitchell, 1987: A $2{\times}CO_2$ climate sensitivity experiment with a global climate model including a simple ocean. *J. Geophys. Res.*, **92**, 13315-13343.

Figure Legends:

FIG. 1. Latitude-height diagram of the zonally averaged annual mean cloud cover (in percents) for $LMD4^{CO}$ (top) and $LMD4^{MO}$ (bottom).

FIG. 2. Same as in Figure 1, but for the cloud liquid water content (0.001 g kg^{-1}).

FIG. 3. Zonally averaged annual mean of the cloud radiative forcing (W m^{-2}) for the infrared radiation (top) and the shortwave radiation (bottom). The curves correspond respectively to $LMD4^{CO}$, $LMD4^{MO}$ and ERBE data for the year 1986.

FIG. 4. (a): Latitude-height diagram of the zonally averaged annual mean of the changes of atmospheric humidity (g kg^{-1}) ($LMD4^{MO} - LMD4^{CO}$). (b) Vertically integrated water vapor content (kg m^{-2}) in function of latitude for respectively $LMD4^{CO}$, $LMD4^{MO}$ and observation (solid line) (Oort 1983).

FIG. 5. Annual mean surface temperature changes (°C) ($1\times CO_2$-$1\times CO_2$p) in $LMD4^{CO}$ (top) and $LMD4^{CO}$ (bottom).

FIG. 6. Temporal evolution (in function of the simulated year) of the global mean surface temperatures (°C): $LMD4^{CO}$ (top); $LMD4^{MO}$ (bottom).

FIG. 7. Changes of the annual and zonal mean surface albedo (%) due to a doubling of CO_2 for $LMD4^{CO}$ and $LMD4^{MO}$.

FIG. 8. Changes of the annual mean surface temperature (°C) due to a doubling of CO_2 for $LMD4^{CO}$ (top), $LMD4^{MO}$ (middle) and an increased solar constant experiment (bottom).

FIG. 9. Changes of the annual mean precipitation (mm day^{-1}) due to a doubling of CO_2 for $LMD4^{CO}$ (top) and $LMD4^{MO}$ (middle). The lower panel indicates the changes of the annual mean precipitation normalized by the inter-annual variability.

FIG. 10. Time-latitude diagram for the changes of surface temperature (°C, left panel) and precipitation (mm day^{-1}, right panel) in $LMD4^{MO}$.

FIG. 11. Latitude-height diagram for temperature changes (°C) (zonally averaged annual mean) ($2\times CO_2 - 1\times CO_2$) for $LMD4^{CO}$ (top) and $LMD4^{MO}$ (bottom).

FIG. 12. Same as in Figure 11, but for the changes of atmospheric specific humidity (g kg^{-1}).

FIG. 13. Same as in Figure 11, but for the relative changes of specific humidity (%).

FIG. 14. Same as in Figure 11, but for the changes of cloud cover (%).

FIG. 15. Same as in Figure 11, but for the changes of cloud liquid (or ice) water content (0.001 g kg^{-1}).

FIG. 16. Streamline function showing the atmospheric meridional circulation for July in LMD4^{CO}: $1\times CO_2$ (top); $2\times CO_2$ (bottom).

FIG. 17. Zonal means (W m^{-2}) of the direct forcing and the feedbacks at the top of the atmosphere for LMD4^{CO} (top) and LMD4^{MO} (bottom).

TABLE 1. Annual and global means for surface temperature (T_s), precipitation (P), atmospheric humidity (q), cloud liquid water content (q_l), cloudiness (C) and surface albedo (α).

model	LMD4^{CO}			LMD4^{MO}		
simulation	1×CO_2	2×CO_2	Δ	1×CO_2	2×CO_2	Δ
T_s (°C)	16.06	19.96	3.9	15.35	18.97	3.6
P (mm day^{-1})	3.23	3.48	0.25	3.56	3.73	0.17
q (kg m^{-2})	25.31	33.26	7.95	23.96	30.91	6.95
q_l (g m^{-2})	46.76	46.58	-0.18	77.80	83.08	5.28
C (%)	70	68	-2	71	70	-1
α (%)	13.15	12.70	-0.45	13.40	12.75	-0.65

TABLE 2. Surface warming (°C) splited into terms of direct forcing and feedback effects.

experiment	$LMD4^{CO}$	$LMD4^{MO}$
$2{\times}CO_2$ forcing	0.64	0.61
water vapor	2.52	2.26
cloud	0.62	0.42
surface albedo	0.12	0.31
total	3.9	3.6

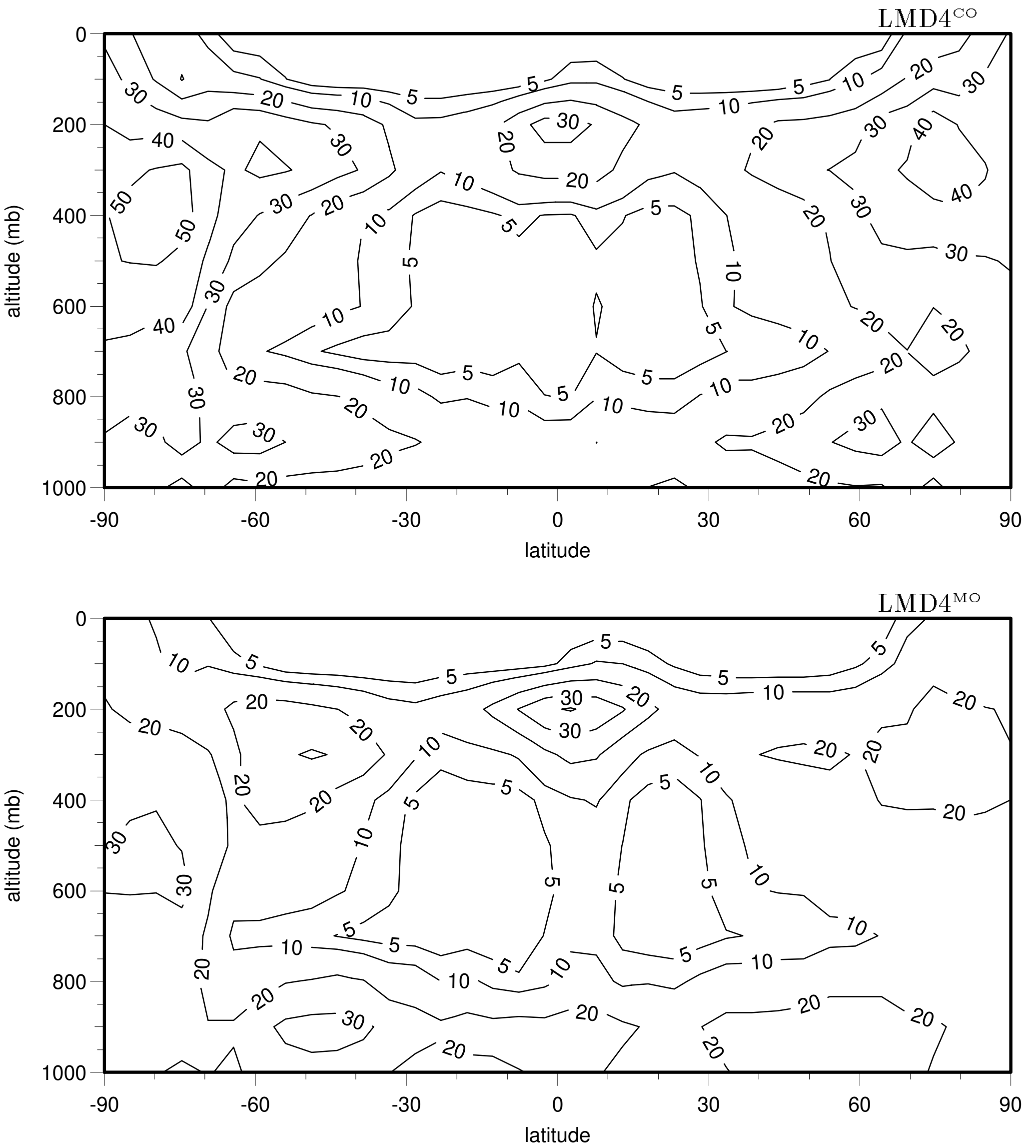
LMD4^{CO}
altitude (mb)
0
200
400
600
800
1000
-90
-60
-30
0
30
60
90
latitude
LMD4^{MO}
altitude (mb)
latitude

Figure 1:

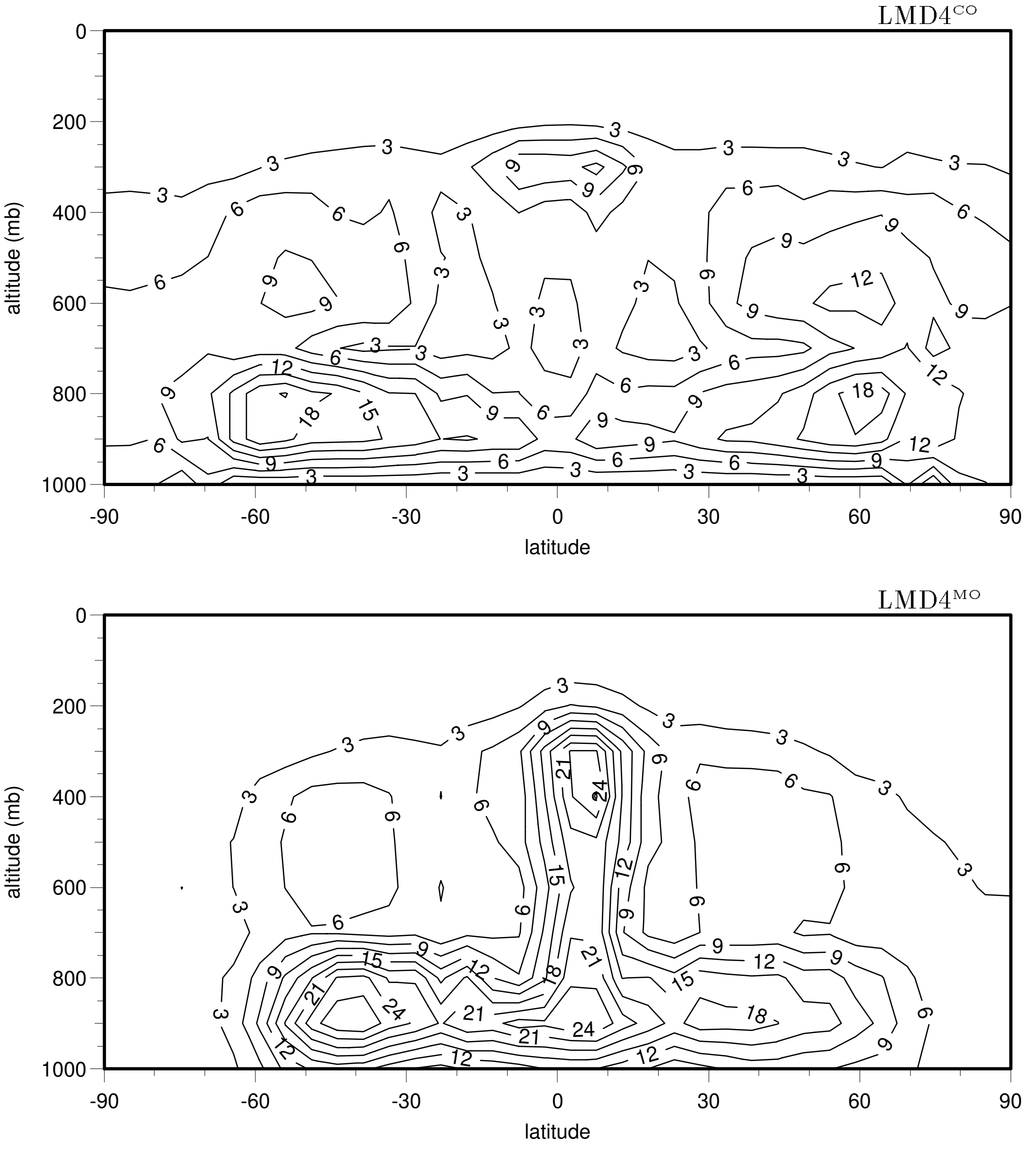

Figure 2:

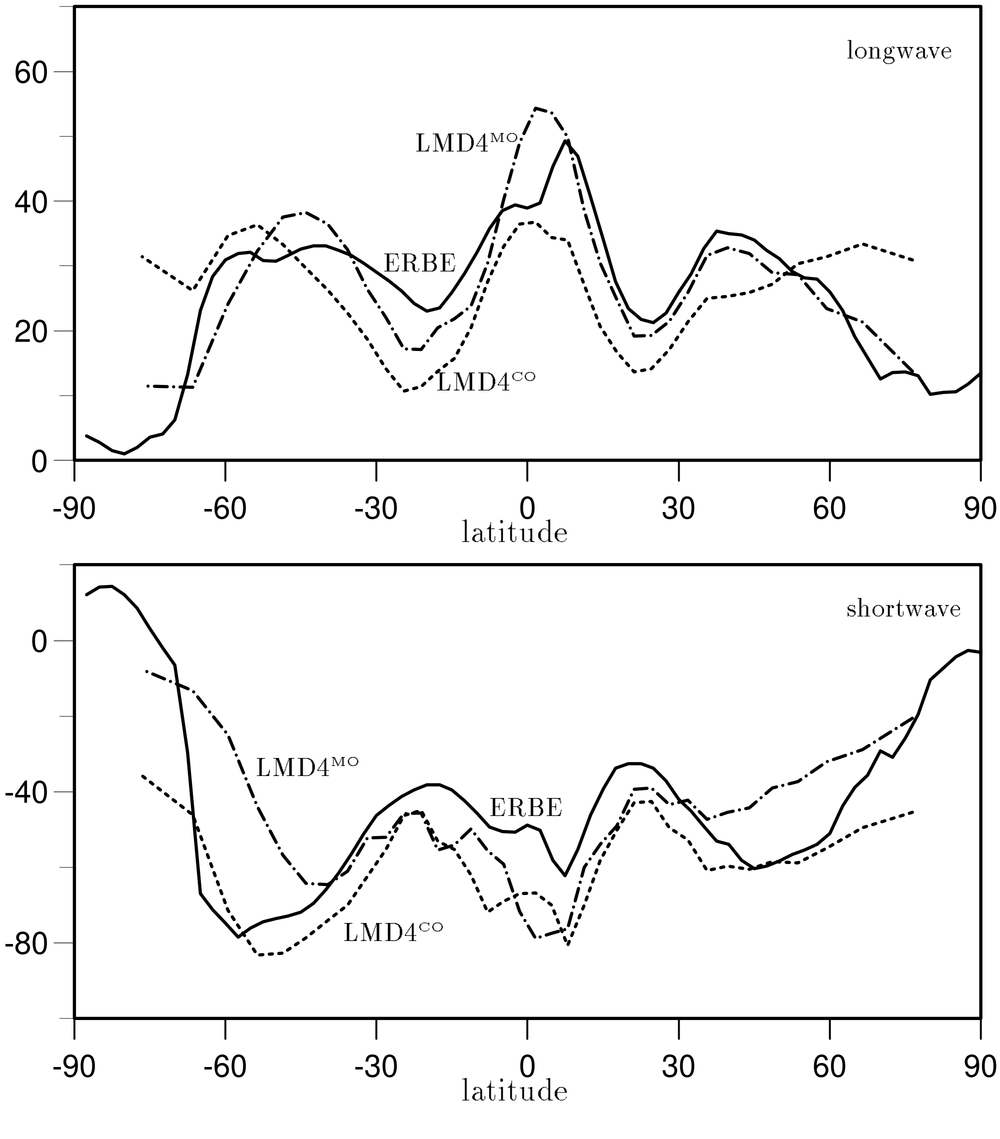
longwave
LMD4^{MO}
ERBE
LMD4^{CO}
60
40
20
0
-90
-60
-30
0
30
60
90
latitude
shortwave
LMD4^{MO}
ERBE
LMD4^{CO}
0
-40
-80
-90
-60
-30
0
30
60
90
latitude

Figure 3:

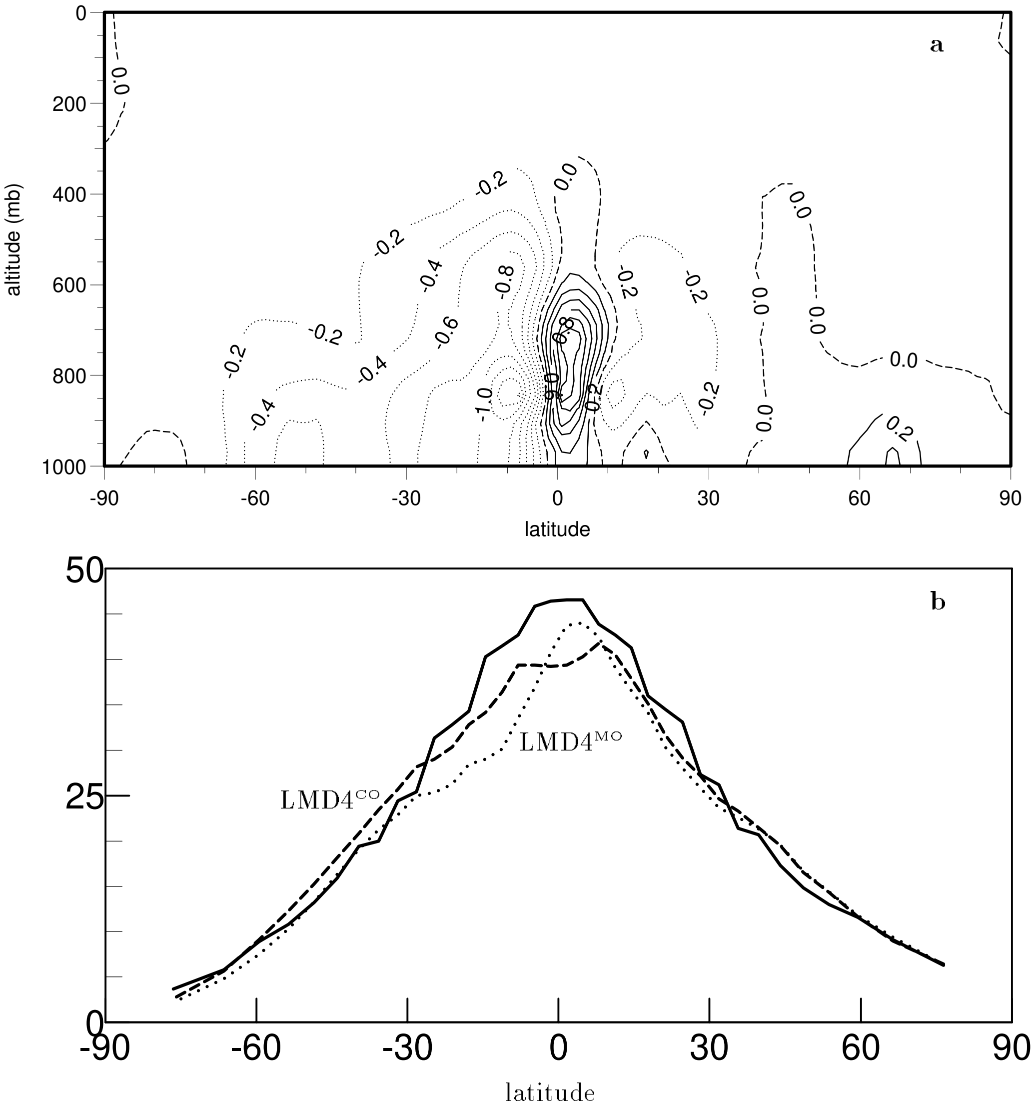

Figure 4:

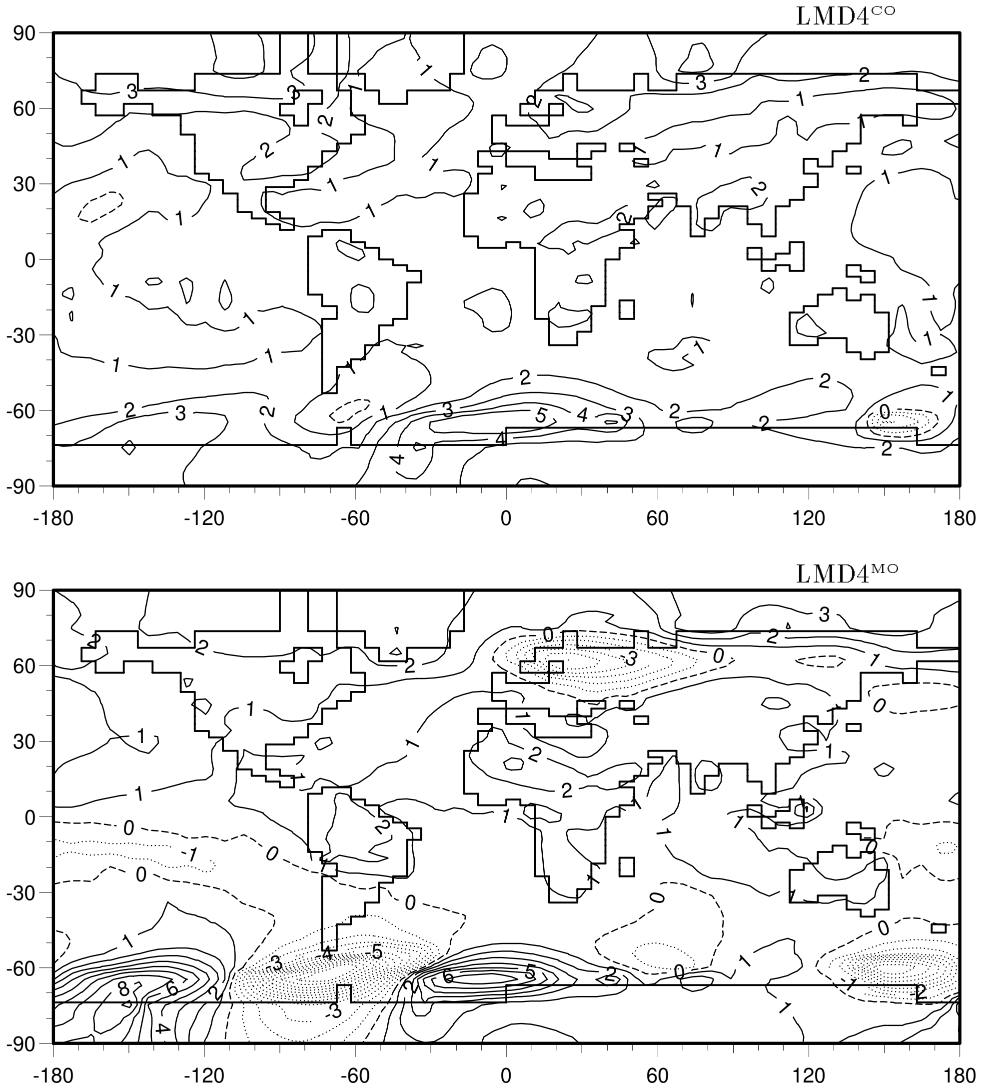

Figure 5:

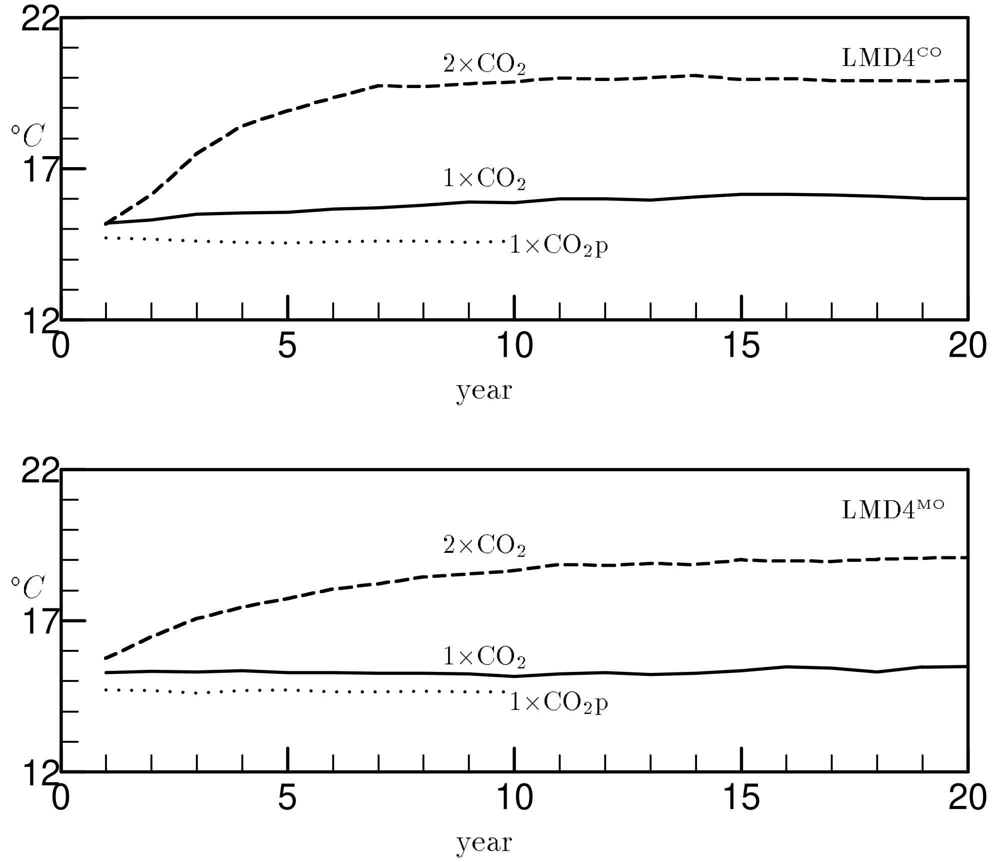
22
17
12
°C
2×CO2
1×CO2
1×CO2p
LMD4CO
0
5
10
15
20
year
22
17
12
°C
2×CO2
1×CO2
1×CO2p
LMD4MO
0
5
10
15
20
year

Figure 6:

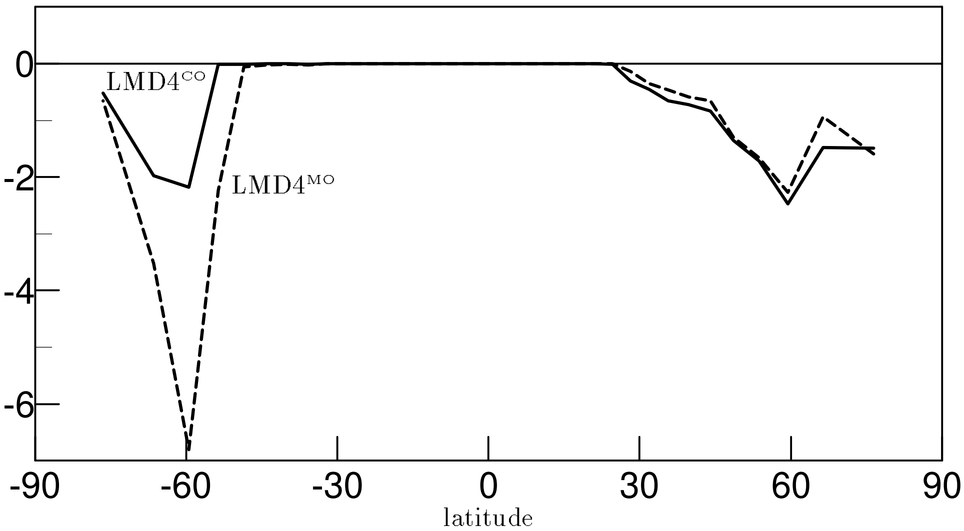

Figure 7:

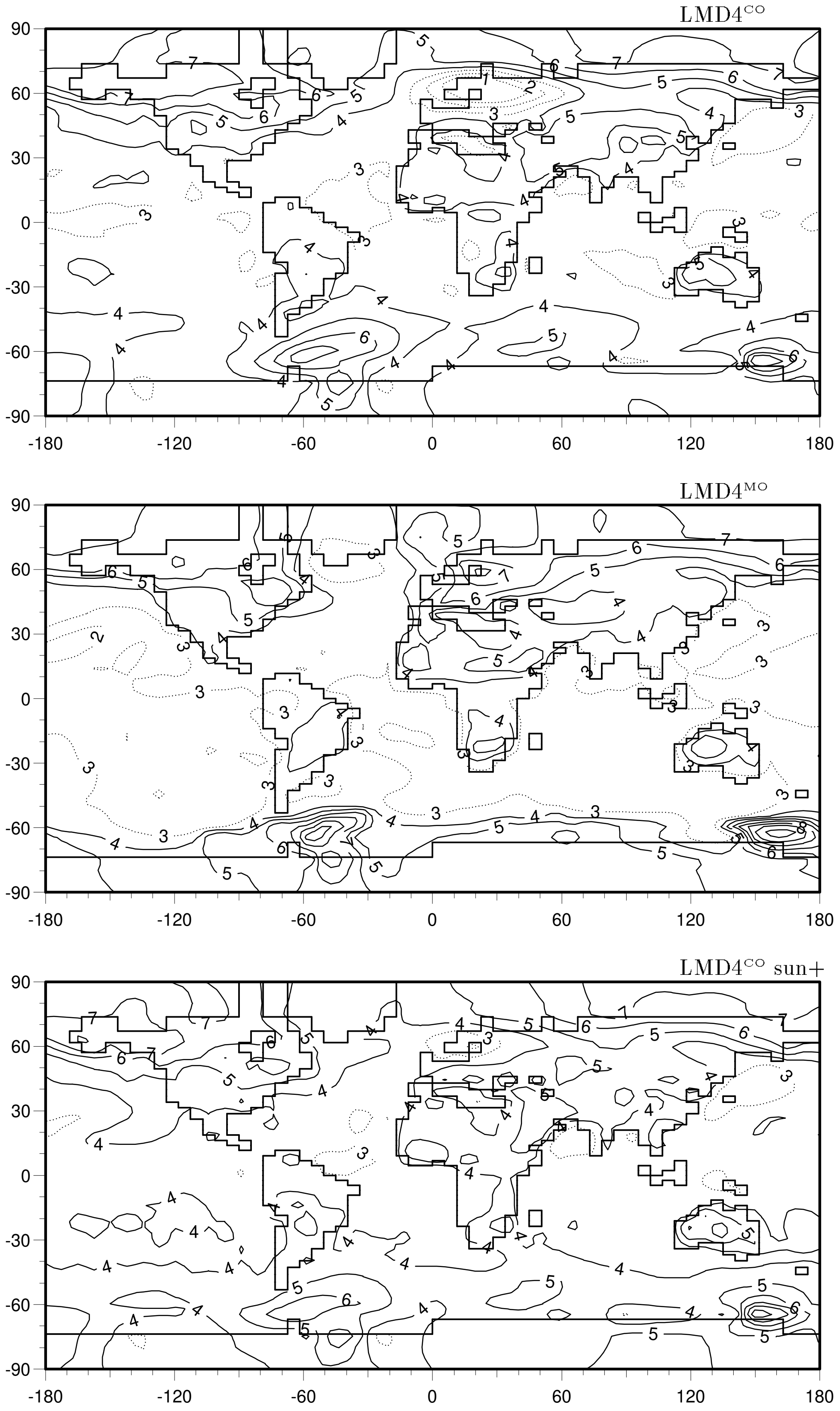
LMD4^{CO}
LMD4^{MO}
LMD4^{CO} sun+
90
60
30
0
-30
-60
-90
-180
-120
-60
0
60
120
180

Figure 8:

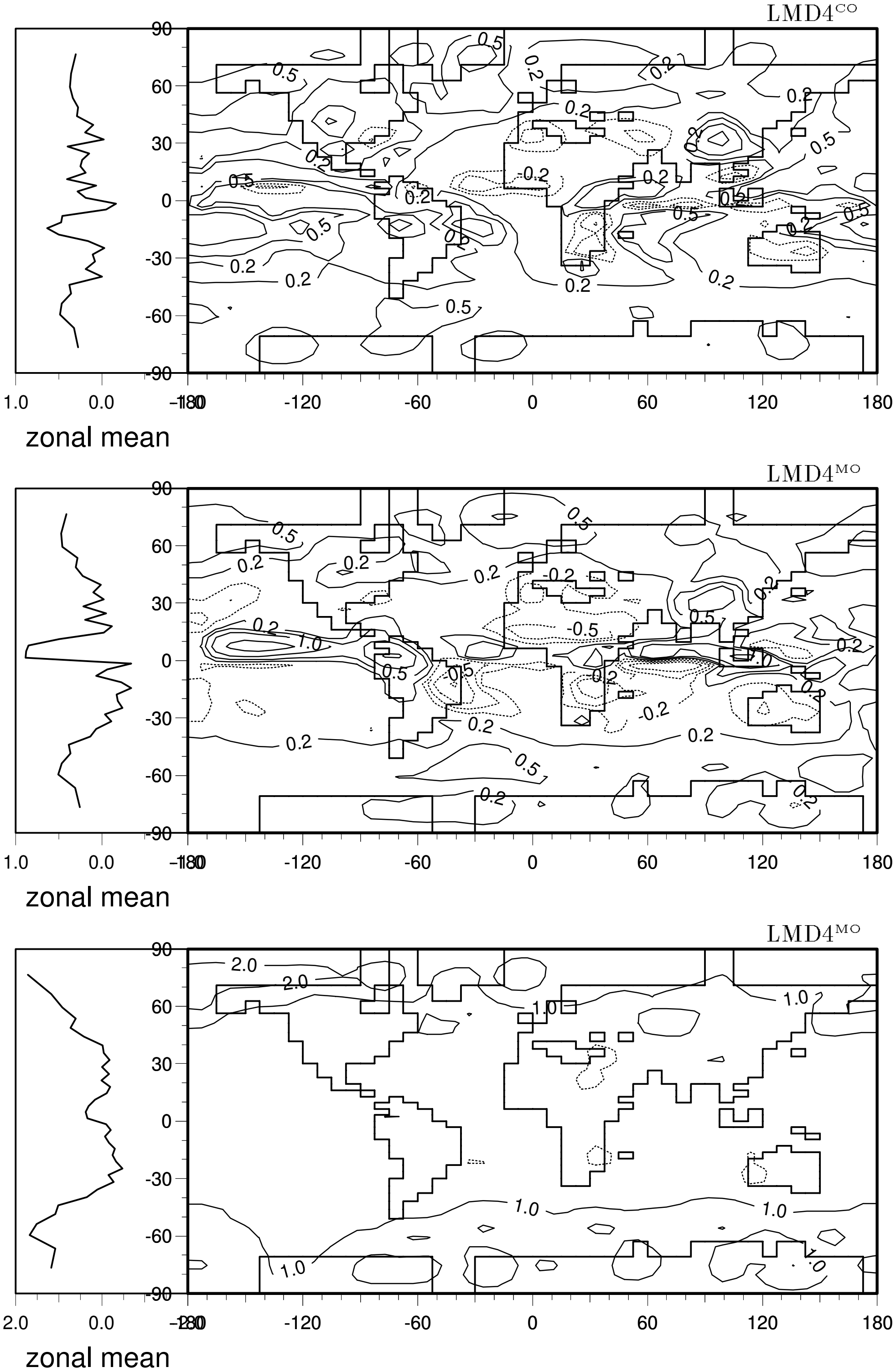
LMD4CO
zonal mean
LMD4MO
zonal mean
LMD4MO
zonal mean
90
60
30
0
-30
-60
-90
1.0
0.0
2.0
-180
-120
-60
0
60
120
180

Figure 9:

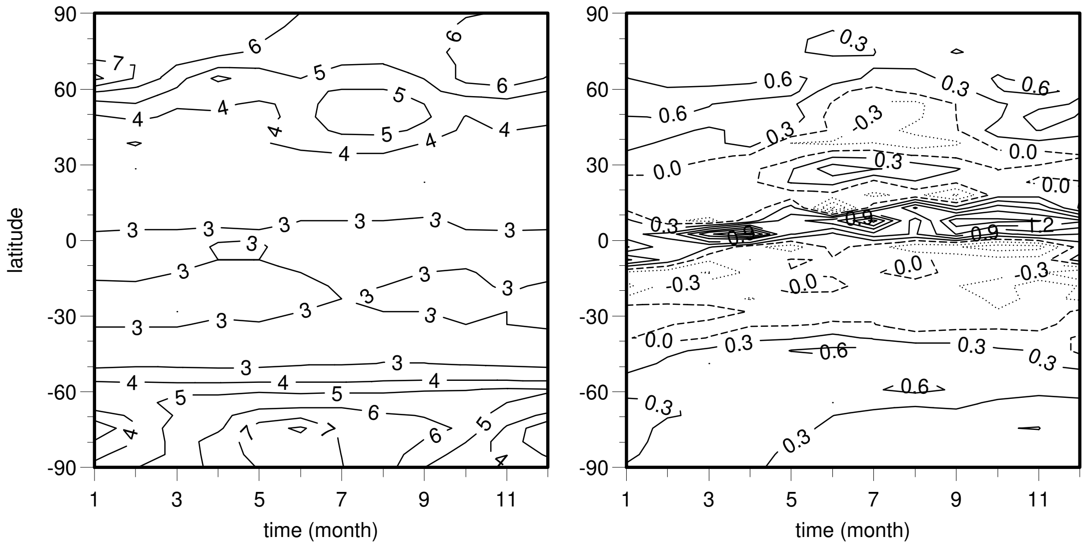

Figure 10:

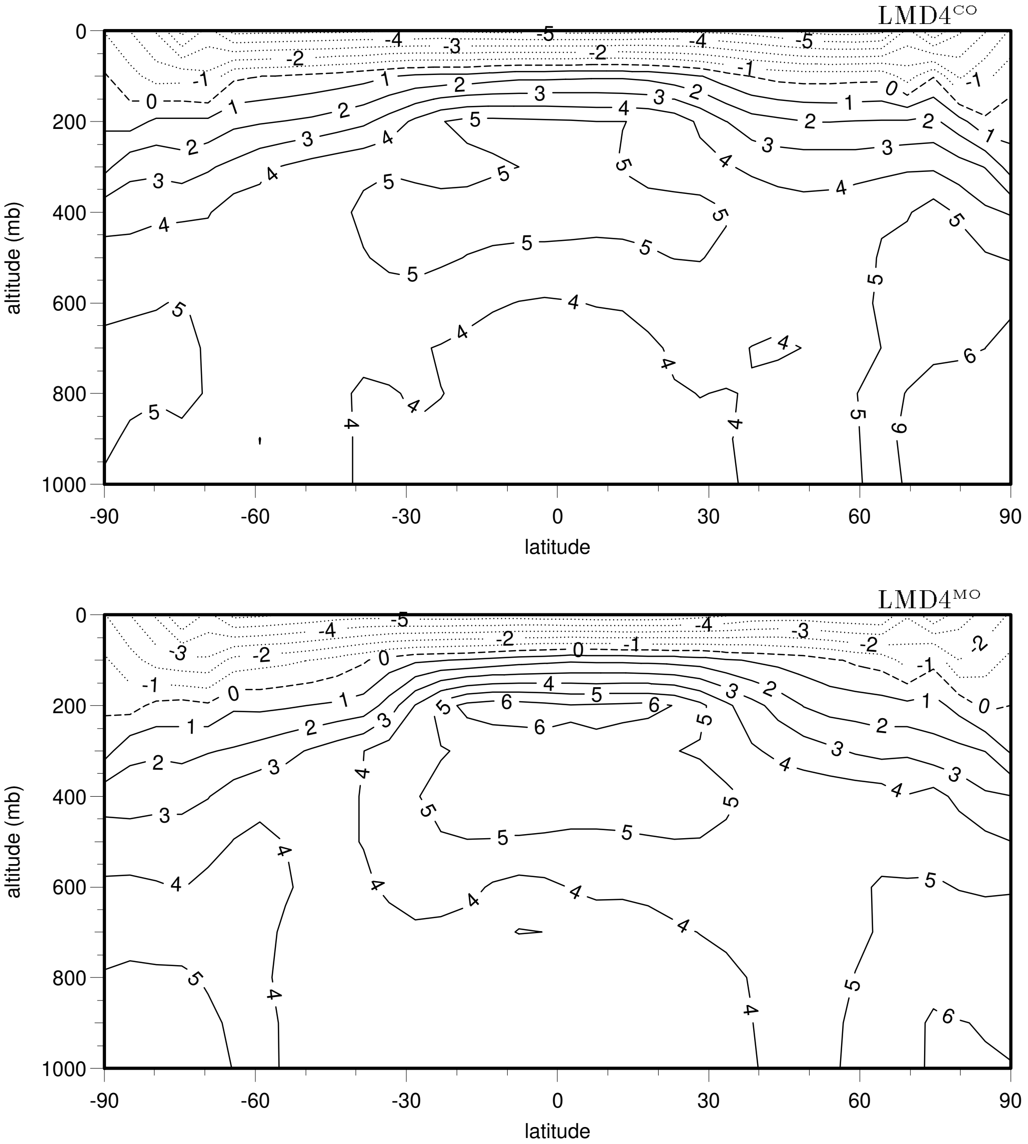

Figure 11:

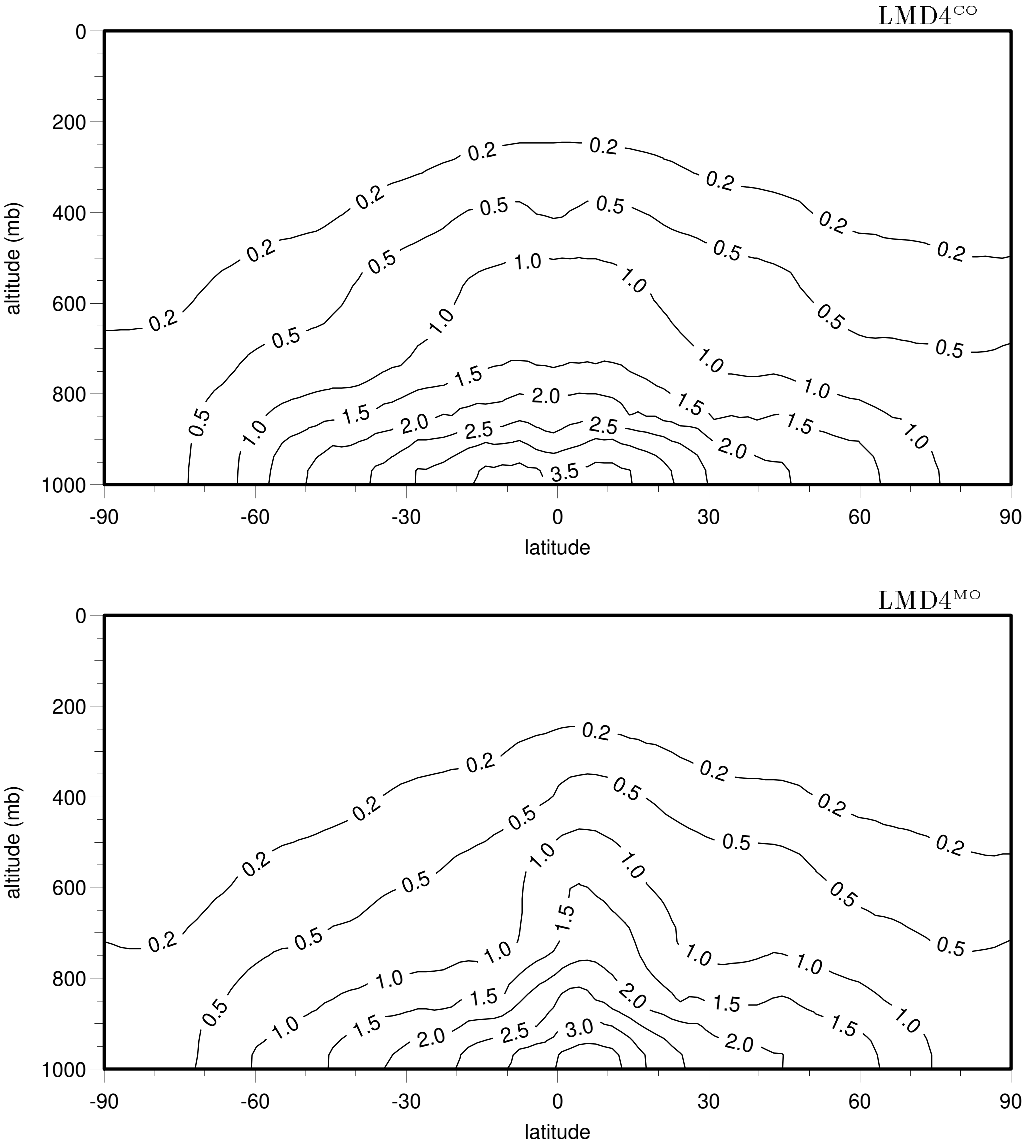

Figure 12:

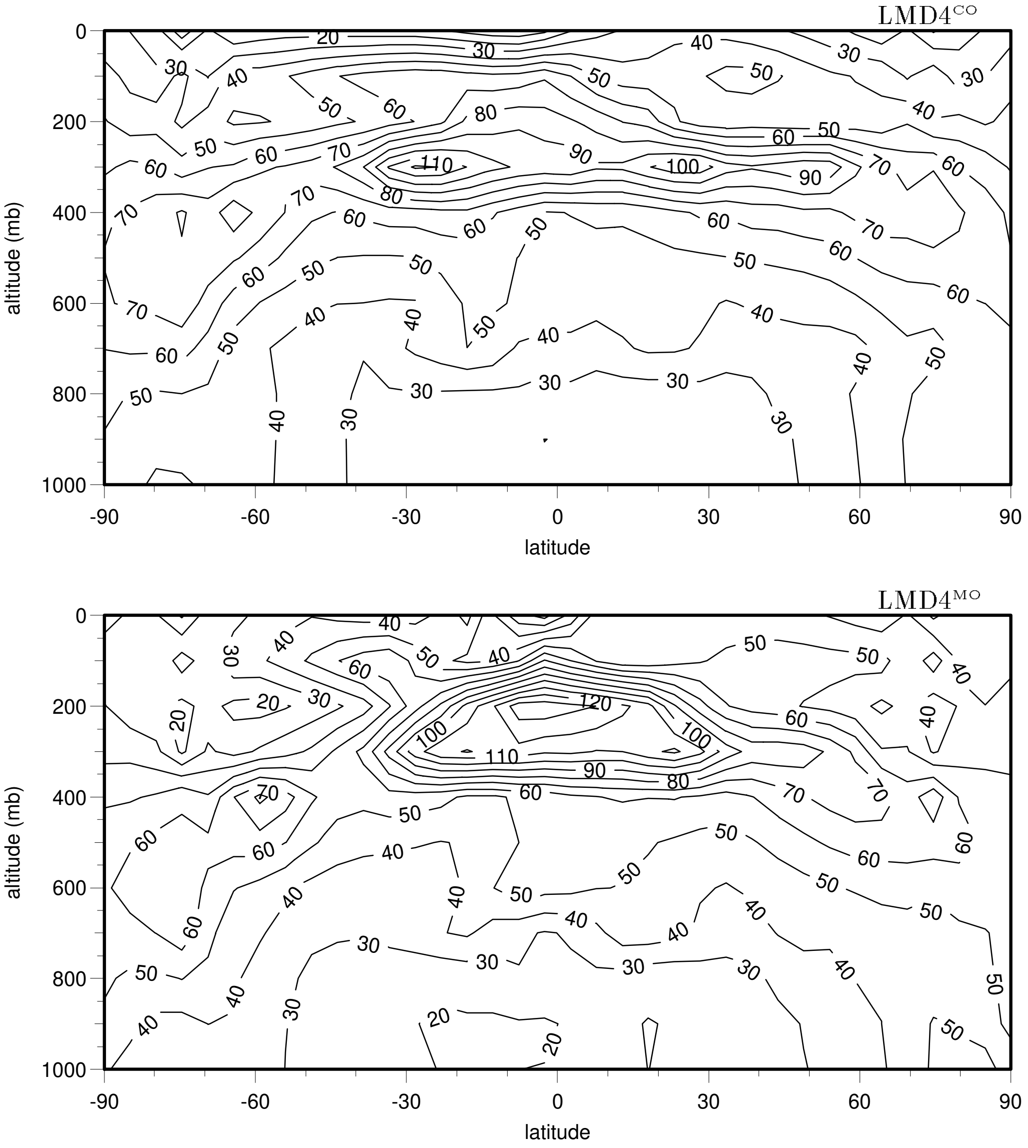

Figure 13:

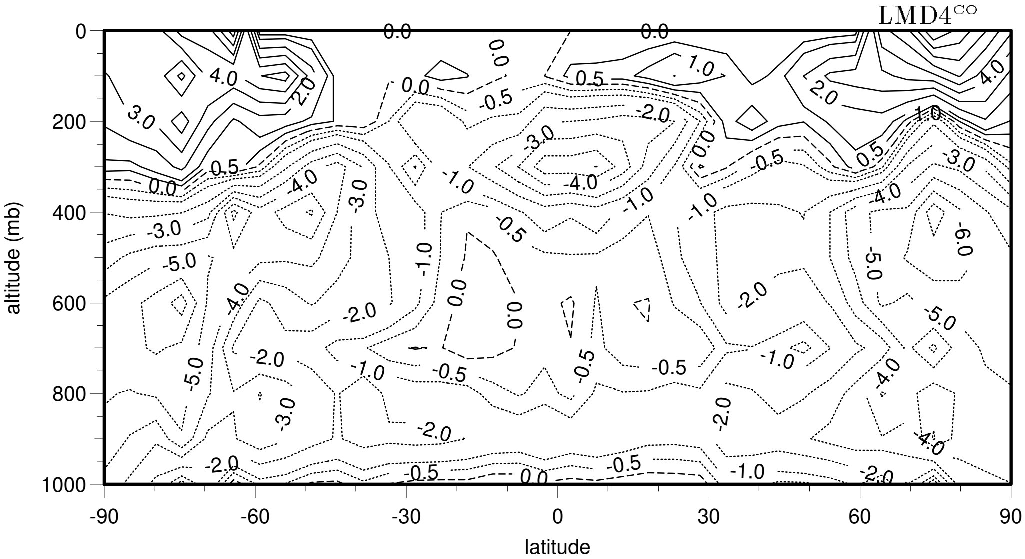

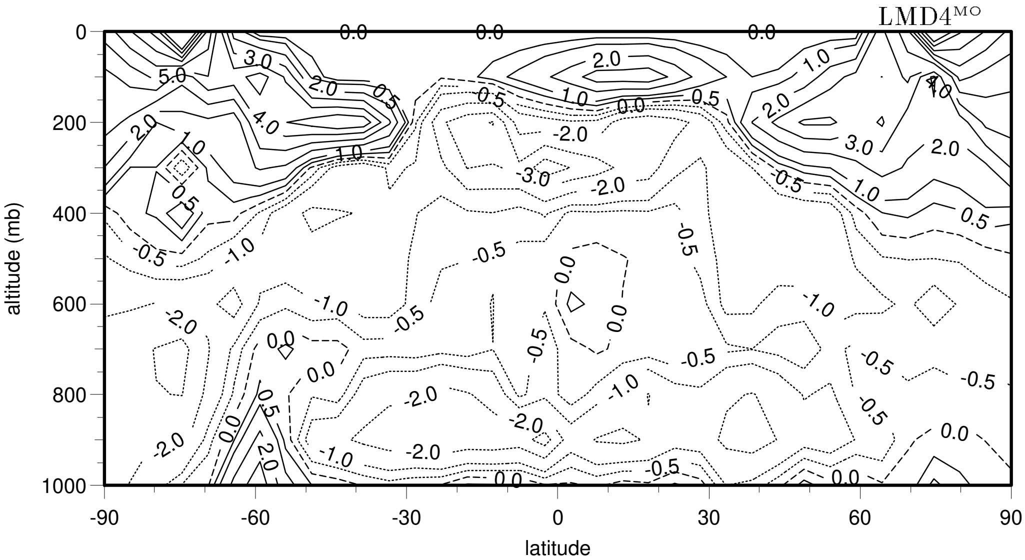

Figure 14:

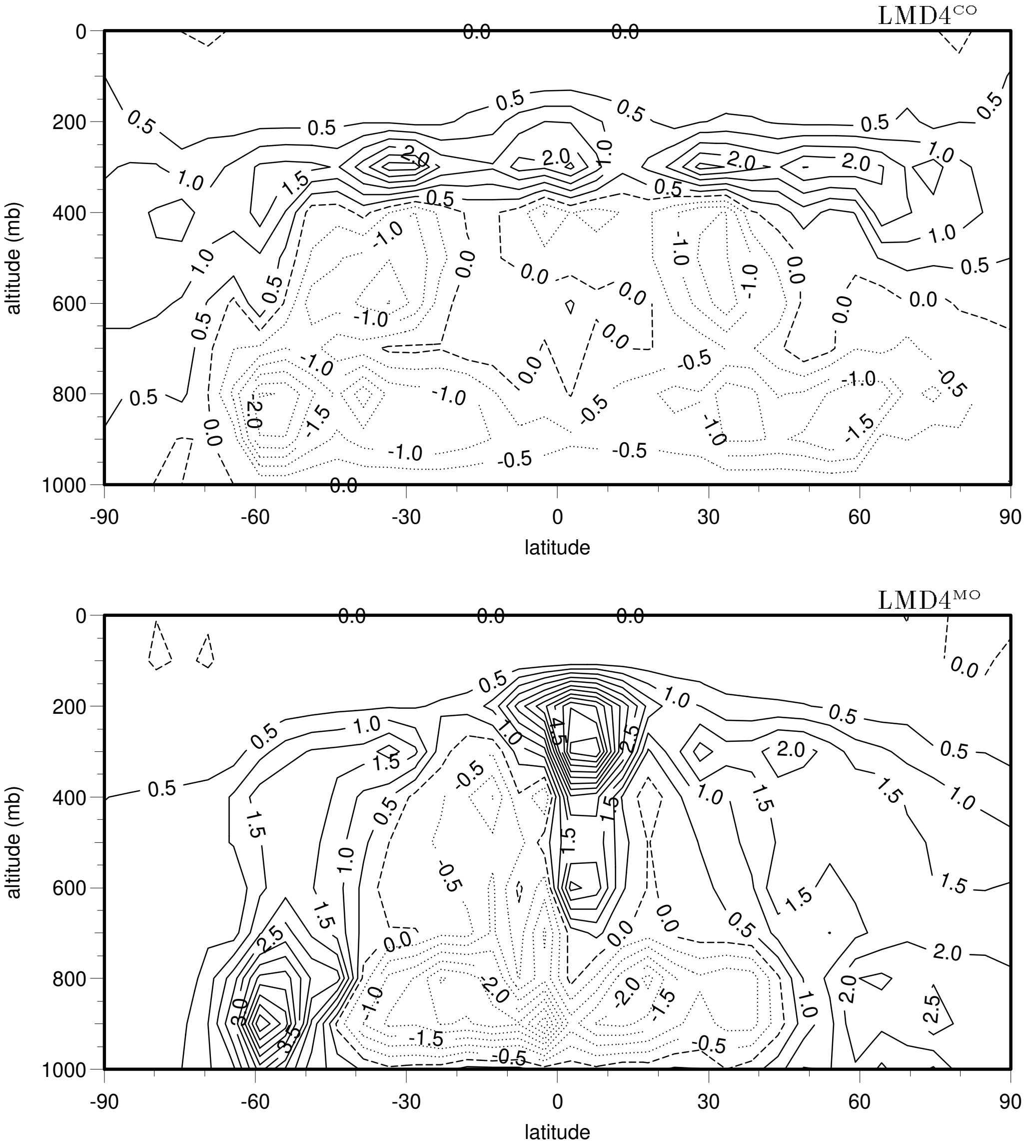
LMD4^CO
altitude (mb)
0
200
400
600
800
1000
-90
-60
-30
0
30
60
90
latitude
LMD4^MO
altitude (mb)
latitude

Figure 15:

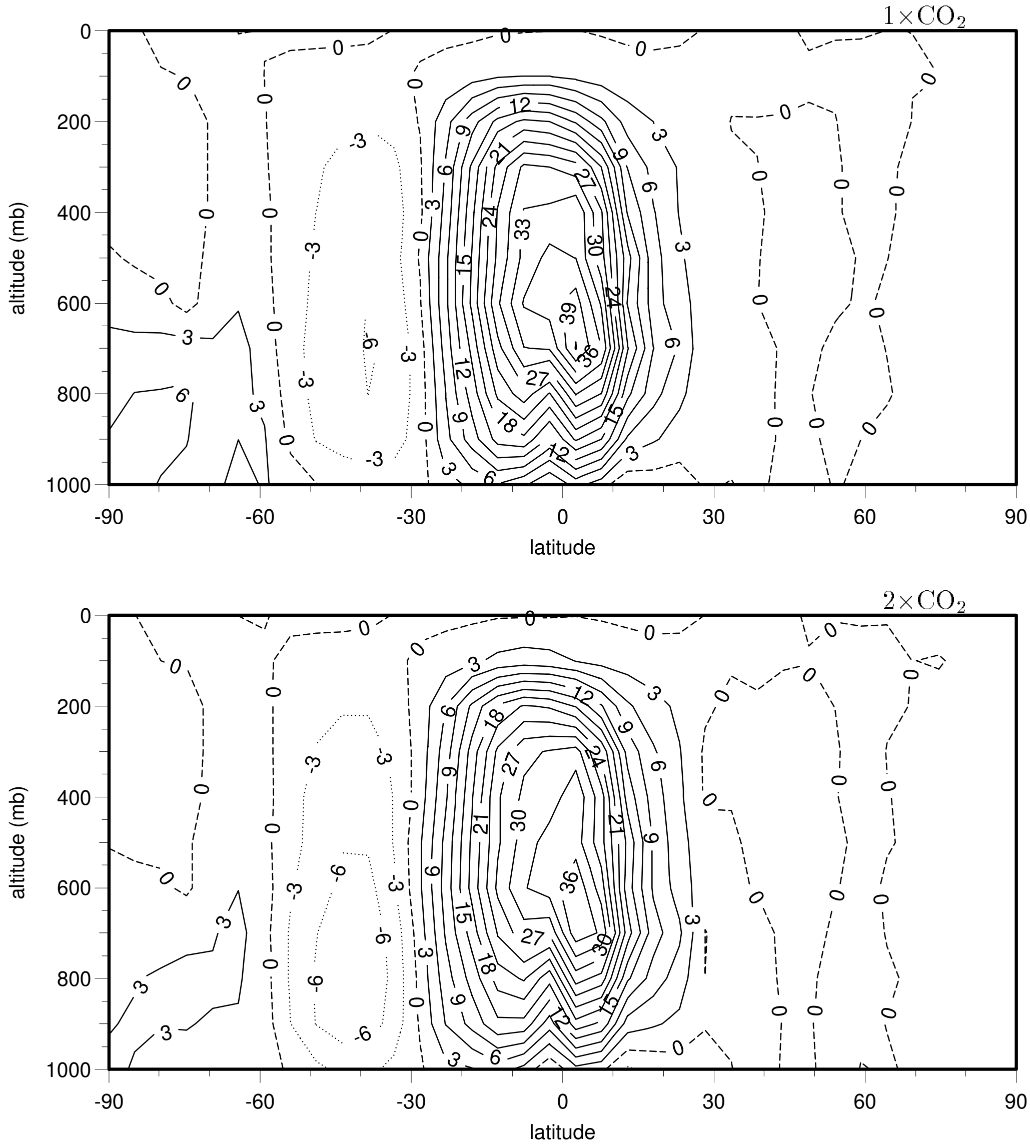

$1\times CO_2$
altitude (mb)
latitude
$2\times CO_2$
altitude (mb)
latitude

Figure 16:

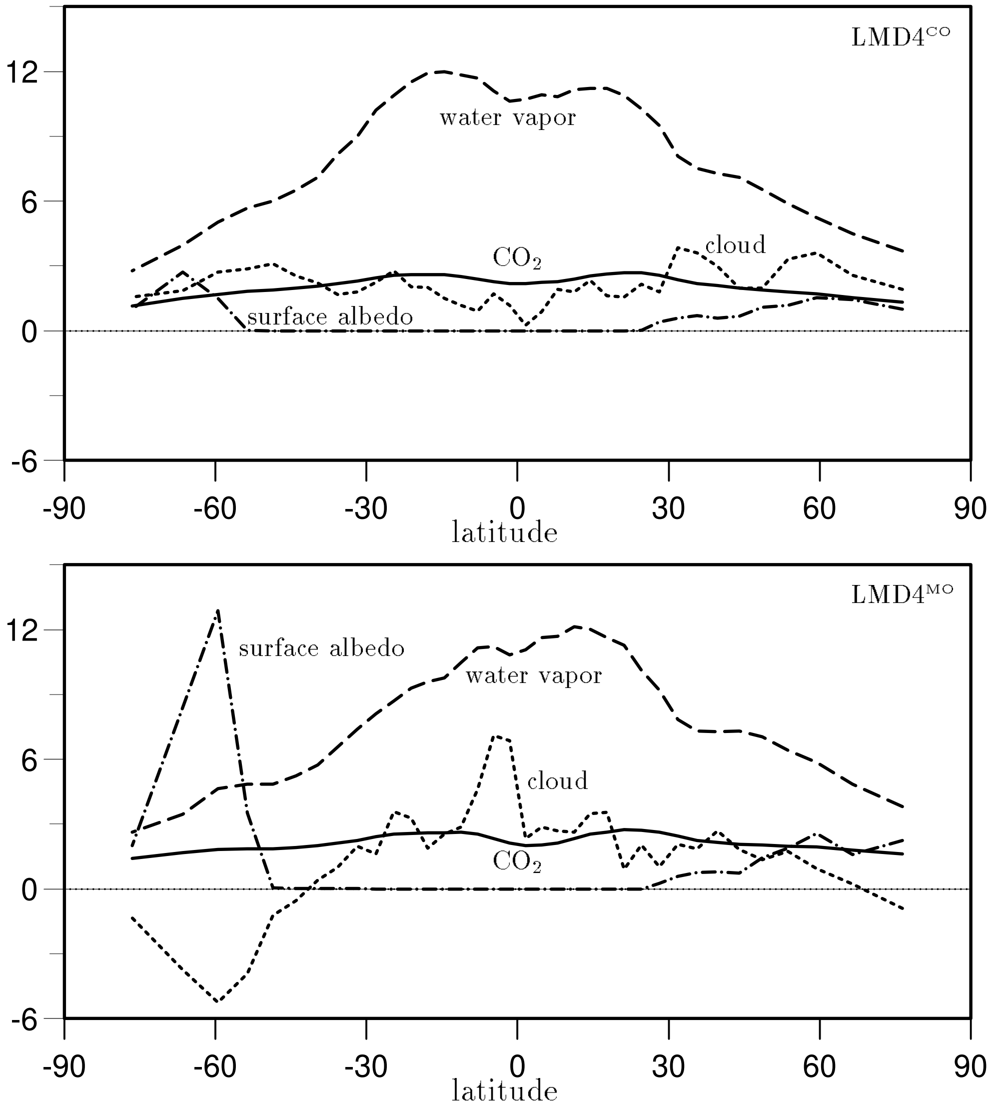

LMD4^{CO}
water vapor
CO_2
cloud
surface albedo
12
6
0
-6
-90
-60
-30
0
30
60
90
latitude
LMD4^{MO}
surface albedo
water vapor
cloud
CO_2
12
6
0
-6
-90
-60
-30
0
30
60
90
latitude

Figure 17: